

2013

Regulation of anoikis by oncogenic pathways

Sun Hee Park

Follow this and additional works at: <https://researchrepository.wvu.edu/etd>

Recommended Citation

Park, Sun Hee, "Regulation of anoikis by oncogenic pathways" (2013). *Graduate Theses, Dissertations, and Problem Reports*. 6375.

<https://researchrepository.wvu.edu/etd/6375>

This Dissertation is protected by copyright and/or related rights. It has been brought to you by the The Research Repository @ WVU with permission from the rights-holder(s). You are free to use this Dissertation in any way that is permitted by the copyright and related rights legislation that applies to your use. For other uses you must obtain permission from the rights-holder(s) directly, unless additional rights are indicated by a Creative Commons license in the record and/ or on the work itself. This Dissertation has been accepted for inclusion in WVU Graduate Theses, Dissertations, and Problem Reports collection by an authorized administrator of The Research Repository @ WVU. For more information, please contact researchrepository@mail.wvu.edu.

Geotechnical Laboratory Testing for 2-D FEM Analysis of Geomorphic and Planar
Sloped Caps and Covers for Sustainable Mine Refuse Deposition

Rogan D. Park

Thesis submitted to the
Benjamin M. Statler College of Engineering and Mineral Resources
at West Virginia University

in partial fulfillment of the requirements for the degree of

Master of Science
in
Civil and Environmental Engineering

John D. Quaranta, Ph.D., P.E., Chair
Leslie C. Hopkinson, Ph.D.
Hema J. Siriwardane, Ph.D., P.E.

Department of Civil and Environmental Engineering

Morgantown, West Virginia
2017

KEYWORDS: GLD, geomorphic, conventional planar, isotropic consolidated undrained (ICU), modeling, seepage, infiltration, factor of safety

Copyright 2017 Rogan D. Park

ABSTRACT

Geotechnical Laboratory Testing for 2-D FEM Analysis of Geomorphic and Planar Sloped Caps and Covers for Sustainable Mine Refuse Deposition

Rogan D. Park

This thesis reports the findings of the application of Geomorphic Landform Design principles to the Royal Scot abandoned coarse coal refuse (CCR) pile located in Greenbrier County, West Virginia. The Royal Scot facility has many environmental concerns including severe erosion, acid-mine/rock drainage, and sediment transport. A cap and cover system is proposed to be implemented which incorporates the GLD principles.

A two-layer cap and cover system will be used to reclaim the site and return it back to a stable state and reduce the production of acid-mine drainage. The system is composed of a hydraulic barrier composed of compacted CCR, and a compacted 80%/20% mixed growth layer. The 80/20 layer is composed of 80% CCR and 20% MGroTM material. The MGroTM is a short paper fiber material produced by the WestRock[®] paper mill in Covington, Virginia. This material provides the characteristics to allow for the growth of grass on the Royal Scot site. A suite of geotechnical laboratory testing was performed including, classification of the coarse coal refuse, compaction, permeability, and strength testing. The results showed that the compacted CCR could perform as a hydraulic barrier to reduce infiltration into the pile, and the strength for slope stability. The permeability of the CCR was in the magnitude of 10^{-6} to 10^{-7} cm/s, and the friction angle for CCR resulted in 25 degrees. The 80/20 growth layer had a permeability of 10^{-4} cm/s to allow water for growth, while the friction angle ranged from 10 to 16 degrees.

Finite Element Modeling was performed on a geomorphic and conventional planar slope located on the site to analyze the cap and cover system for slope stability. The analysis consisted of seepage modeling, coupled with slope stability to get a worst-case scenario factor of safety after infiltration from a 100-year storm event had occurred. The geomorphic slope had increased infiltration compared to the conventional planar slope. The geomorphic slope produced higher factors of safety over 2.0, while the conventional planar slope attained factors of safety close to 1.5.

Table of Contents

ABSTRACT.....	ii
Table of Contents.....	iii
List of Figures.....	iv
List of Tables.....	v
Introduction/Background.....	1
Purpose.....	4
Objective.....	4
Scope of Work.....	4
Literature Review.....	5
Materials and Methods.....	7
Results.....	12
Grain Size Distribution.....	12
Compaction Testing.....	14
Hydraulic Conductivity Testing.....	16
Triaxial Compression Strength Testing.....	20
Summary of Geotechnical Laboratory Testing Results.....	28
Numerical Modeling.....	32
Modeling Methodology.....	32
Modeling Inputs.....	35
Modeling Results.....	37
Conclusions and Recommendations.....	49
References.....	50

List of Figures

Figure 1. Location of Royal Scot site and several other coal refuse facilities (Stevens, 2016).....	1
Figure 2. Cross-section of previous proposed growth layer and hydraulic barrier (Stevens, 2016)	2
Figure 3. Image of typical MGro™ sample.....	3
Figure 4. Display of the ICU triaxial test.....	9
Figure 5. Grain Size Distribution for CCR.....	13
Figure 6. Compilation of compaction test results	15
Figure 7. Hydraulic conductivity vs. pore volume plot for standard compacted CCR (592.5 kJ/m ³)	17
Figure 8. Hydraulic conductivity vs. pore volumes for 11% compacted 80%/20% CCR/MGro™ blend (67.85 kJ/m ³).....	19
Figure 9. p-q plot for standard compacted CCR (592.5 kJ/m ³)	20
Figure 10. Stress-Strain plot for standard compacted CCR (592.5 kJ/m ³)	21
Figure 11. p-q plot for 11% compacted 80/20 CCR/MGro™ blends (67.85 kJ/m ³)	23
Figure 12. Stress-Strain plot for 11% Compacted 80%/20% CCR/MGro™ blend (67.85 kJ/m ³)	24
Figure 13. p'-q' plot for 11% compacted 80/20 CCR/MGro™ blend (67.85 kJ/m ³).....	26
Figure 14. Pore-water pressure versus axial strain for 11% compacted 80/20 CCR/MGro™ blend (67.85 kJ/m ³).....	28
Figure 15. Image of Royal Scot plan including the location of slope profiles that are modeled (Adapted from Lorimer, 2016)	32
Figure 16. Day 3-Conventional Planar Slope (Ditch G) saturation with streamlines.....	38
Figure 17. Day 4-Conventional Planar Slope (Ditch G) saturation with streamlines.....	39
Figure 18. Day 15-Conventional Planar Slope (Ditch G) saturation with streamlines.....	39
Figure 19. Day 25-Conventional Planar Slope (Ditch G) saturation with streamlines.....	40
Figure 20. Day 3-Geomorphic Slope (GLD-C) saturation with streamlines	41
Figure 21. Day 4-Geomorphic Slope (GLD-C) saturation with streamlines	42
Figure 22. Day 15-Geomorphic Slope (GLD-C) saturation with streamlines	42
Figure 23. Day 25-Geomorphic Slope (GLD-C) saturation with streamlines	43
Figure 24. Mean factor of safety/critical area for conventional planar slope (Ditch G).....	45
Figure 25. Mean factor of safety/critical area for geomorphic slope (GLD-C).....	46

List of Tables

Table 1. Geotechnical material properties tests	4
Table 2. List of Geotechnical testing values for CCR	6
Table 3. Testing conditions for standard compacted CCR (592.5 kJ/m ³)	10
Table 4. Critical Indices for Grain Size Distribution	13
Table 5. USCS Soil Classification	14
Table 6. Summary of compaction test results	14
Table 7. Hydraulic Conductivity testing results for standard compacted CCR (592.5 kJ/m ³)	16
Table 8. Hydraulic Conductivity results for 11% Proctor 80%/20% CCR/MGro TM blend (67.85 kJ/m ³)	18
Table 9. Consolidated Undrained friction angle results for standard compacted CCR (592.5 kJ/m ³)	22
Table 10. Summary statistics for friction angle results (standard compacted CCR) (592.5 kJ/m ³)	22
Table 11. Consolidated Undrained friction angle results for 11% Compacted 80%/20% CCR/MGro TM blends (67.85 kJ/m ³)	25
Table 12. Summary statistics for friction angle results (11% Compacted 80%/20% CCR/MGro TM blends) (67.85 kJ/m ³)	25
Table 13. Consolidated Undrained friction angle results for 11% compacted 80/20 blend (67.85 kJ/m ³)	27
Table 14. Parameter summary table for Geotechnical lab testing	29
Table 15. Probabilistic storm data for modeling	33
Table 16. Boundary condition locations	33
Table 17. Soil Water Characteristic Curve (SWCC) Parameters	35
Table 18. SVFlux TM input parameters for modeling	36
Table 19. 3-Sigma friction angle values	36
Table 20. SVSlope® input parameters for modeling	37
Table 21. Saturation of growth layer and hydraulic barrier	38
Table 22. Saturation of growth layer and hydraulic barrier	41
Table 23. Quantitative seepage/stability analysis for conventional planar slope (Ditch G)	44
Table 24. Quantitative seepage/stability analysis for geomorphic slope (GLD-C)	44

Introduction/Background

This study investigates the comparative differences between two primary amended soil designs for use in covering and capping the Royal Scot site located in Greenbrier County, West Virginia. This site is a bond forfeiture abandoned mine refuse site. The research performed consists of a geotechnical laboratory investigation on two amended refuse blends, and implement the geotechnical data into a two-dimensional (2D) Finite Element Modeling analysis consisting of slope stability coupled with seepage analysis. The two amended refuse specimens analyzed consisted of coarse coal refuse (CCR), and an 80%/20% CCR/MGro™ blend material. The site is composed of an old abandoned coarse coal refuse facility. A map of the location of the Royal Scot site can be seen below in Figure 1 along with several other coal refuse facilities. The site has been abandoned since 1999 and exhibits many environmental issues (Ward, 2001). Some of these environmental issues consist of severe channel erosion and increased acid mine drainage. Royal Scot site has little to no vegetation, and uses a passive treatment facility to treat the acid mine drainage that leaches from the refuse fill.

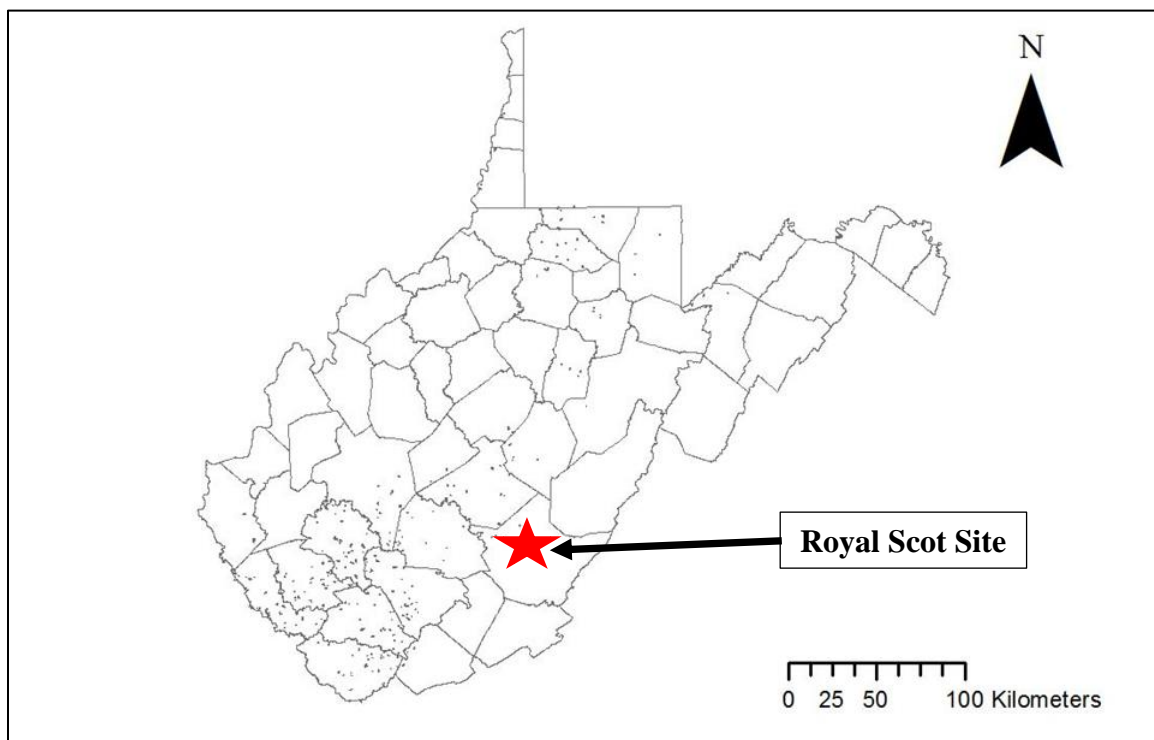


Figure 1. Location of Royal Scot site and several other coal refuse facilities (Stevens, 2016)

The site reclamation is proposed to be reclaimed by the West Virginia Department of Environmental Protection (WVDEP) following the geomorphic landform design (GLD) principle approach. GLD attempts to mimic the natural equilibrium of erosive forces found in mature

landforms (Schor and Gray, 2007). As opposed to conventional reclamation techniques, GLD requires less maintenance and are more geotechnically stable (Nicolau, 2003). The motivation for this study was to use unsaturated 2D finite element modeling to gauge how the seepage/stability affects a GLD slope designs compared to conventional planar faced slopes with bench cut profiles.

The Royal Scot site has a previous proposed 60/40 CCR/MGroTM cap and cover design (Stevens, 2016). This system was composed of three layers including a fill material, compacted hydraulic barrier, and growth layer. The site also went under a hydraulic regrade design that included ditches for drainage of water, and GLD channels to reroute water to its corresponding watershed (Lorimer, 2016). The geometry from the hydraulic regrade could be accessed and used in the modeling procedure. The system was composed of three layers including a fill material, compacted hydraulic barrier, and growth layer. A cross-section of the previous proposed growth layer and hydraulic barrier can be seen in Figure 2. All layers are made up of coarse coal refuse (CCR). The CCR fill material will be the base of the cover, and then compacted CCR is used as the hydraulic barrier. The proposed cap and cover design uses a hydraulic barrier measuring 2 feet in thickness across the entire site for the GLD slopes, and a 2 to 1-foot taper will be used from the crest to the toe of the conventional planar slope (Stevens, 2016). The upper part of the cap and cover system is the growth layer. The proposed growth layer is made up of 60% coarse coal refuse and 40% MGroTM material and is 1 foot thick across the entire site for this analysis.

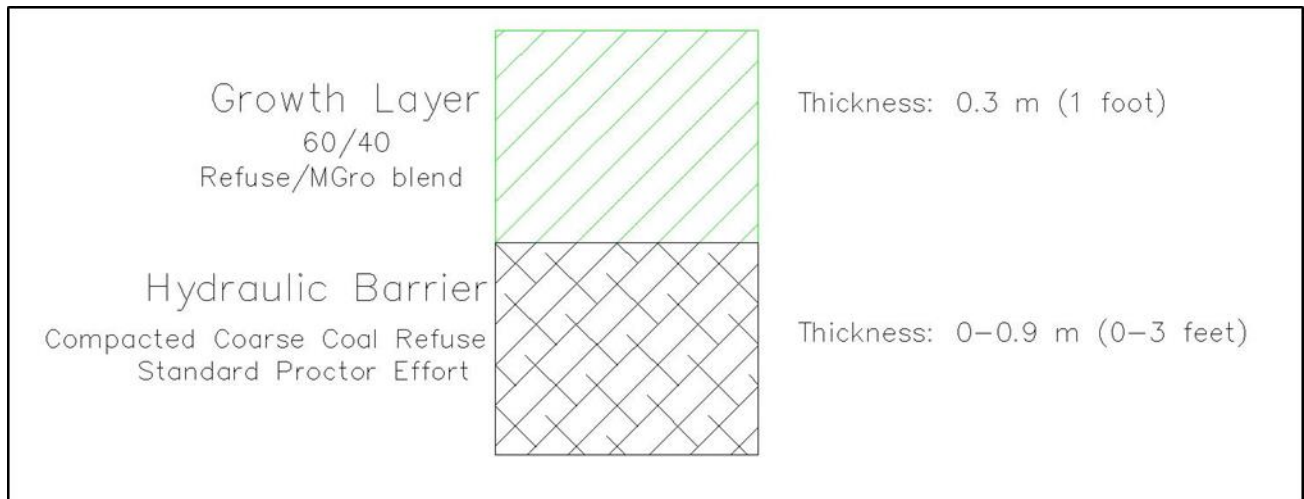


Figure 2. Cross-section of previous proposed growth layer and hydraulic barrier (Stevens, 2016)

As mentioned, MGroTM is used in the growth layer for the cap and cover design. MGroTM is a byproduct from a paper mill located in Covington, Virginia produced by WestRock[®]. The material is created by solid residuals produced by the treatment of paper mill and carbon plant wastewater. Its composition is 85% solids from primary clarification of mill wastewater and 15%

microbial biomass from biological wastewater treatment. MGro™ was also evaluated and recommended by (Daniels et al. 2013) as a soil amendment. An image of the MGro™ material is shown in Figure 3.



Figure 3. Image of typical MGro™ sample

Since 2010 West Virginia University's Department of Civil and Environmental Engineering has researched geomorphic landform design (GLD) for application in Central Appalachia. Some of the accomplishments include conceptual GLD on a permitted valley fill; geotechnical slope stability evaluation of GLDs for steep terrain; evaluation of differences in groundwater seepage between conventional planar and geomorphic landform designs; and comparisons of hydrologic response (DePriest, 2015). The goal of this projects is to evaluate the use of GLD for Appalachian coal field reclamation, and determine if the approach is cost effective for the region. If proven successful, the citizens and State of West Virginia will benefit from GLD model through reduced environmental impact, improved water quality, and improved flood control.

Purpose

The purpose of this research is to optimize an alternative cap blend ratio mixture for the reclamation of a coarse coal refuse pile located in central Appalachia. An 80/20 CCR/MGro™ growth blend will be analyzed for economic savings and performance compared to a previous proposed 60/40 CCR/MGro™ growth blend. The goal of this research is to reduce construction costs and reduce seepage into the refuse pile due to the generation of acid rock drainage/acid mine drainage into nearby streams originating from the Royal Scot refuse site.

Objective

The objective of this study is to perform laboratory testing on refuse and MGro™ blend specimens, and evaluate that data to perform computer based Finite Element Modeling (FEM). Slope stability and seepage modeling will be done to gauge performance criterion. The results from the computer modeling can be used to quantify design values to compare with the proposed cap and cover design.

Scope of Work

The scope of work is separated into three tasks.

Task 1-Geotechnical Lab Testing

Geotechnical laboratory testing was performed on two specimen types. The first specimen is coarse coal refuse which is found on the Royal Scot site. The second specimen is the 80/20 CCR/MGro™, which is proposed as an alternative cap and cover system to the proposed design. Laboratory testing was performed on these two specimens to obtain their geotechnical index and performance properties for comparative analysis. Table 1 presents the testing procedure performed and its corresponding American Society of Testing Materials protocol.

Table 1. Geotechnical material properties tests

Test Name	ASTM
Grain Size Distribution (GSD)	D-422
Compaction	D-698
Hydraulic Conductivity	D-5084
Triaxial Isotropic Consolidated Undrained Strength (ICU)	D-4767

Task 2-2D Finite Element Analysis

Task 2 involves performing 2-D analysis on a conventional planar and geomorphic slope profile. After completion of the laboratory testing, the properties are used for Finite Element Modeling. The modeling will involve assessment of infiltration/seepage and slope stability to gauge the cap and cover system performance.

Task 3-Evaluation of Results

The last task is to evaluation of the Finite Element Analysis. Evaluating the modeling involves analysis of saturation/pore water pressure, infiltration into the slope profile, and if the slopes are stable under a worst-case scenario storm. This involves comparing/contrasting the modeling to the proposed design to determine if acid mine drainage can be reduced.

Literature Review

Geomorphic Landform Design

Geomorphic landform design (GLD) is a new landforming technique that has become prominent in mine reclamation. The studies for GLD began in the early 2000's (Nicolau, 2003). GLD differs from conventional landforming in terrain profile, stability, and erosion/water management. Conventional landforms typically consist of steep slope profiles with benches to alleviate driving forces. GLD profiles implement the principle of geomorphology to create a terrain that is similar to its former natural landform (Nicolau, 2003).

Research has also shown that GLD slopes have higher factors of safety in regard to slope stability. Russell et al. (2014) performed slope stability analysis on geomorphic and conventional slope profiles in Southern West Virginia. The geomorphic profiles proved to have higher factors of safety (2.04-3.49) compared to conventional designs (1.25-1.67). Russel et al. (2014) states that the reason for increased stability in geomorphic slopes is due to its shallow profiles compared to steep profiles that are prevalent in conventional slopes.

Another study on GLD was performed in Southern West Virginia on erosion/water management by DePriest et al. (2015). The study was performed on steep terrain that mimic a surface mine site. The geomorphic designs showed potential for decreased erosion, and improvement of water management/transport on the site according to DePriest et al. (2015).

Short Paper Fiber

Short paper fiber (SPF) is a by-product from water treatment at paper mills. The material is derived from paper making materials such as wood, fiber, clay, and organic matter. The SPF for this research is produced by WestRock[®] and is marketed as MGro[™]. Recent studies have shown that SPF has the capabilities to be used as a soil amendment. Carpenter and Fernandez (2000) mixed paper mill sludge with topsoil. The combination of the sludge and soil were able to produce vegetative growth. The WestRock[®] MGro[™] has also been able to serve as a vital soil amendment for growth according to Daniels et al. (2003).

SPF blends have been applied in West Virginia for coal refuse reclamation purposes. Laubenstein (2004) used a SPF/topsoil cover along the Tygart River. The blended material was used as the cover material. Water quality greatly improved with the use of the SPF/topsoil cover, and prove to beneficial for coal refuse reclamation purposes (Laubenstein, 2004).

Geotechnical Laboratory Testing

The use of CCR in impoundments/dams dates back to the late 1970's. The refuse is commonly used to construct dams to retain a slurry of fine coal refuse (FCR) and water (Hegazy et al. 2004). These impoundments can be found throughout West Virginia, Pennsylvania, Ohio, Virginia, and Kentucky. Throughout each state the CCR shale varies due to regional geologic conditions, and coal mining/preparation processes (D'Appolonia, 2009). A list of geotechnical testing for index and strength for CCR can be seen in Table 2.

Table 2. List of Geotechnical testing values for CCR

Coarse Coal Refuse (CCR) Laboratory Testing Values						
Reference	Location	Grain Size				Effective Shear Strength
		D ₃₀ (mm)	D ₅₀ (mm)	D ₆₀ (mm)	Passing 200 Sieve (%)	φ' (degrees)
Almes and Butail (1976)	PA, WV, KY, VA	0.7	2.5	4.5	10	33-39
McCutcheon (1981)	OH	1.9	4.5	7	7	36
Saxena et al. (1984)	WV	12	16	22	2	27-40
Albuquerque (1994)	VA	3.5	7.5	12	1.5	39
Hegazy et al. (2004)	PA	0.35	1.23	2.02	19.8	34

As mentioned CCR varies due to its regional geography and processes it undergoes. Table 2 shows values for grain size that vary greatly. According to Hegazy et al. (2004), 19.8% passed the #200 sieve, which classifies as clays/silts. This is much larger than what was seen in the other research as all other CCR testing showed less than 10% passed the #200 sieve. This large increase in fines is accredited to advances in coal mining and preparation processes over the last 15 years, which resulted in a trend toward greater percentages of fines in CCR (D'Appolonia, 2009). Table 2 also shows effective shear strength friction angle values for different regions. The data shows that CCR is variable when it comes to friction angle. In West Virginia, the angle can range from 27-40 degrees, which is highly variable. (Saxena et al. 1984). The other regions show that the friction angle varies from 33 to 39 degrees.

Materials and Methods

As mentioned in Task 1, geotechnical lab testing was performed on two separate soil specimens. Coarse coal refuse (CCR) and MGro™ were the two materials that underwent lab testing. The testing was done according to the most recent ASTM standards. Table 1 shows the ASTM standards and their corresponding designation. The goal of the geotechnical laboratory testing was to gain the two materials geotechnical indexes and performance properties to compare to previous studies.

Grain Size Distribution

The first set of testing was acquiring the grain size distribution (GSD) of the CCR shale material. GSD was done according to ASTM D-422. The material that was analyzed was CCR obtained from the Royal Scot site. The soil was obtained using a ¾ in. sieve (19 mm opening) in the field. The GSD allows gives useful indexes such as the coefficient of uniformity (C_u) and coefficient of gradation (C_c). These indexes allow the CCR to be classified into its United Soil Classification System (USCS) soil classification.

Compaction Testing

Compaction testing was the next testing procedure to gain the unit weights of CCR and the 80/20 blend material. Compaction testing was performed according to ASTM D-698 to find the dry unit weight of two materials. The tests were performed at 11% Standard Proctor compaction (67.85 kJ/m³ compaction energy). The two test that were performed are as follows:

1. Coarse Coal Refuse at 11% Proctor Energy (67.85 kJ/m³ (1,425 ft-lb/ft³))
2. 80%/20% CCR/MGro™ Blend at 11% Proctor Energy (67.85 kJ/m³ (1,425 ft-lb/ft³))

The coarse coal refuse at 11% proctor was completed to find the correct moisture content and dry unit weight so the blend material could be compacted. The blend material was completed on a by volume basis using a one cup vessel for each test (i.e. 20 cups=16 cups CCR+4 cups MGro™). The blend was then mixed in a blender at 11% CCR proctor moisture content.

Hydraulic Conductivity

Hydraulic conductivity testing was performed according to ASTM D-5084 (Flexible Wall permeability testing) for two specimens:

1. Coarse Coal Refuse at Standard Proctor Energy (592.5 kJ/m³)
2. 80%/20% CCR/MGro™ Blend at 11% Proctor Energy (67.85 kJ/m³)

Flexible wall was chosen over rigid wall testing due to the possibility of particle migration that is prevalent in rigid wall permeability.

The standard Proctor CCR was compacted at a target density of 15.9 kN/m³ and 14.3% moisture content, while the growth blend target density was 11.2 kN/m³ and 31.9% moisture. A hydraulic gradient of $i=15$ was used for standard compacted testing. A hydraulic gradient of 15 is not

recommended by ASTM, but was needed to accelerate the time of the testing procedure. A hydraulic gradient of $i=15$ was also used to achieve the same accelerated testing for the growth blend. Triplicate testing was done for both standard compacted, and 11% compacted samples to ensure accuracy. The testing procedure was done until the readings achieved a steady state. Steady state means the parameters were constant and allowed to reach a steady flowrate. Once each test reached a steady state, the hydraulic conductivity could be determined based on the last five measurements that were taken.

Triaxial Strength Testing

For strength testing, isotropic consolidated undrained (ICU) triaxial testing was performed. The specimens that were tested include the standard compacted CCR and 11% compacted 80/20 MGro™ materials. A GeoTac Sigma 1 triaxial device was used for this testing procedure. Figure 4 shows the set-up of the triaxial machine with specimen in flex-wall.

In order to account for pore water pressure build-up in the slopes, consolidated undrained (ICU) tests were run in accordance with ASTM D-4767. ICU triaxial testing simulates a worst-case scenario. This test allows the soil specimen to consolidate under specified stress conditions, and then sheared with drainage valves closed to simulate an undrained state. This may not be the case for the field site, but CU results will give conservative values for analysis.



Figure 4. Display of the ICU triaxial test

Standard Compacted CCR (592.5 kJ/m³)

Standard Proctor Compacted CCR was tested (592.5 kJ/m³) for shear strength under two different confining pressures. The CCR gradation was passing a 19 mm (3/4 in.) sieve which was the same as GSD. These conditions were chosen as a worst-case scenario. The first confining pressure chosen was a middle failure which corresponded to 24.38 m (80.0 feet) into the slope. The second confining pressure simulated a deep failure of 36.58 m (120 feet) into the slope profile. For the two worst-case conditions, a soil density of 15.71 kN/m³ (100 lb/ft³) was used to estimate the stress condition for ICU testing. This density was chosen to simulate the average of different compaction efforts that may likely be found at the Royal Scot site.

Table 3. Testing conditions for standard compacted CCR (592.5 kJ/m³)

Testing Conditions	Depth	Confining Pressure
	m (ft)	kPa (lb/in ²)
1	24.38 (80.0)	386 (56)
2	36.58 (120)	572 (83)

This sweep of isotropic CU testing will be used in the analysis for the hydraulic barrier. The barrier will not be at the specified depths listed in Table 3, but these serve as a conservative estimate to the strength of the CCR at depths found within the site and give insight on how the barrier will perform at a worst-case scenario.

Before the triaxial testing process, the specimens went through permeability testing, so they were near full saturation (61%, 63%, 84%), and no back pressure was done for the CU testing. Bypassing the back-pressure procedure, the specimens went straight from seating to the consolidation phase at the specified confining pressures listed in Table 3. During consolidation, the specimens were under isotropic stress with drainage valves open to allow a change in void ratio.

After completion of isotropic consolidation, the specimens could be sheared. Drainage valves were closed during shearing in accordance with a CU test, allowing no pore water pressure to escape. A constant rate of shear was used with a strain rate of 2% per hour until it reached 20% strain. A pressures sensor was placed on one of the drainage valves to track pore water pressure.

Total Stress Analysis

To calculate friction angles and discover at what strain rate the specimens failed a total stress analysis was used for the standard compacted CCR. For a total stress analysis, stress paths have to be analyzed to discover the materials friction angle and at what strain rate the material failed. The parameters “p” and “q” are defined in equations 1 and 2 for total stress. Equations 1 and 2 are taken from the USACE Manual No. 1110-2-1902 (2003).

$$p = \frac{\sigma_1 + \sigma_3}{2} \tag{Equation 1}$$

$$q = \frac{\sigma_1 - \sigma_3}{2} \tag{Equation 2}$$

Failure Criterion

Sigma 1 and Sigma 3 are defined as the major and minor principal stresses in a Mohr Coulomb plot. Sigma 1 in this testing is the axial stress applied by the piston, and sigma 3 is the confining pressure. The p - q plot is a representation of the center and radius of Mohr's circle and can help calculate the internal angle of friction. Since the material is classified as a coarse sand, cohesion is assumed to be equal to zero.

11% 80/20 CCR/MGro™ (67.85 kJ/m³)

The 11% compacted 80/20 blend underwent the same ICU triaxial testing that the standard compacted CCR underwent, but with much different confining pressures. The blend material had confining pressures of 34.5 and 69 kPa (5 and 10 psi) versus 386 and 572 kPa (56 and 83 psi). These stresses were low as the growth/blend layer is only designed to be one foot thick. These pressures are overestimates as was the standard compacted CCR for worst-case scenario. The four specimens underwent the same permeability testing as the standard compacted CCR to reach near or at full saturation ($i=15$). After completing reaching a steady state hydraulic conductivity, the specimens could then be placed on the triaxial machine to undergo seating and isotropic consolidation at the 34.5 and 69 kPa confining pressure. The test followed the same procedure for shear with the drainage valves closed to not allow any dissipation, and following an “undrained” condition. The same strain rate of 2% per hour until reaching 20% strain was used for the 80/20 testing.

Two different methods of analysis were used to determine friction angle and failure for the 80/20 blends. A total stress analysis was attempted for the 80/20 blends. This was the same method that was used for the standard compacted CCR, but some issues arose with the stress paths, and their behavior, so a new approach was taken. The other method that was used for analysis was an effective stress analysis. The major difference between a total and effective stress analysis is the subtraction of the pore water pressure from the major and minor principal stresses. Equations 3 and 4 show the parameters p' and q' which govern an effective stress analysis. The (') indicates that the major and minor principal stresses (Sigma 1 and Sigma 3) subtract out the pore-water pressure (u) indicating an “effective” stress analysis. Equations 3 and 4 are taken from the USACE Manual No. 1110-2-1902 (2003).

$$p' = \frac{\sigma_1' + \sigma_3'}{2} \quad (\text{Equation 3})$$

$$q' = \frac{\sigma_1' - \sigma_3'}{2} \quad (\text{Equation 4})$$

The reason for using an effective stress analysis is the behavior of MGro™ in the 80/20 blends. As the piston compresses the sample, it is expected the material would also compress. That is not the case with the 80/20 blend. The MGro™ material cause the sample to undergo dilation or it causes the sample to extend as the piston is compressed. The effective stress analysis also allows the lightly compacted blend material to consolidate. The MGro™ portion of the blend, went under isotropic consolidation under a confined pressure. As the sample was confined, water would leave the MGro™ material, but did not have any path due, which would lead to the sample to undergo dilation.

Results

Grain Size Distribution

Figure 5 shows the Grain Size Distribution for the coarse coal refuse shale material. GSDs classify the material on the basis of gravels, sands, silts/clays. The plot lists all particle sizes and the following U.S. Standard Sieve Size. The two tests that were performed show consistent results for GSD 1 and GSD 2 with only small minor differences in the sand portion.

After performing the GSD, the shale material could then be classified according to the United Soil Classification System (USCS)-ASTMD-2487. The two GSD tests performed show that the material was on the border of a gravel and sand. Over 50% of the material passes the #4 sieve classifying it as a sand. The gradation curve also shows that there are less than 5% fines and greater than 15% gravel classifying the material as well graded sand with gravel (SW), but is on the verge of being poorly graded due to the coefficient of gradation.

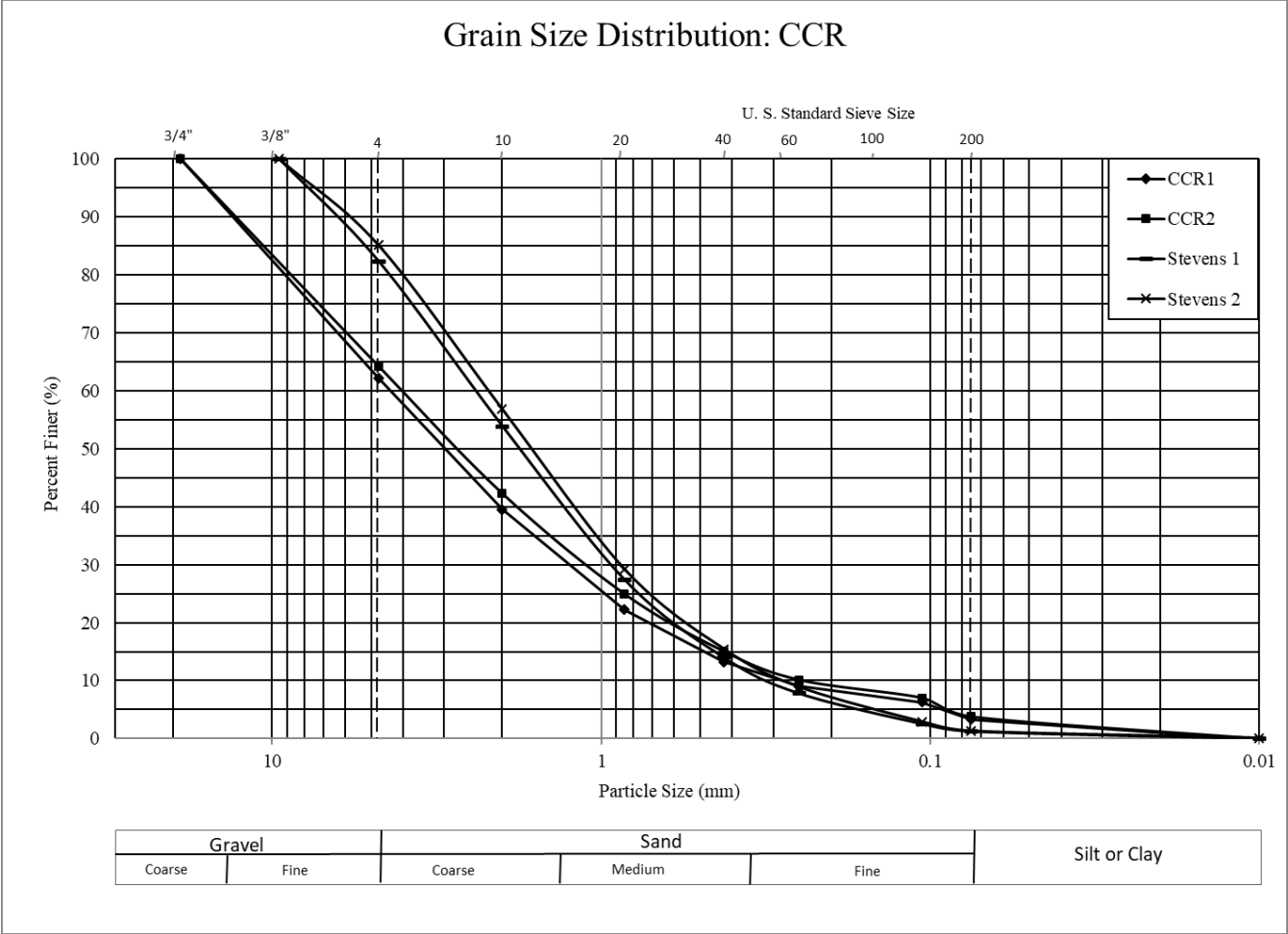


Figure 5. Grain Size Distribution for CCR

Table 4. Critical Indices for Grain Size Distribution

Results	CCR1	CCR2	Average
D₉₀ (mm)	10.40	10.40	10.40
D₆₀ (mm)	4.40	4.00	4.20
D₅₀ (mm)	3.00	2.90	2.95
D₃₀ (mm)	1.40	1.20	1.30
D₂₅ (mm)	1.00	0.85	0.93
D₁₀ (mm)	0.29	0.27	0.28
Cu-Coefficient of Uniformity	15.17	14.81	14.99
Cc-Coefficient of Gradation	1.54	1.33	1.43

Table 5. USCS Soil Classification

USCS Soil Classification	Group Symbol
Well graded sand with gravel	SW

Compaction Testing

Table 6 gives a summary of the optimum dry unit weight and corresponding moisture contents. A compilation of the compaction curves is given in Figure 6 with zero air void lines and 90% saturation lines for each compaction curve.

Table 6. Summary of compaction test results

Compaction Energy	Optimum Dry Unit Weight (kN/m³)	Optimum Moisture Content (%)
CCR 11% Proctor (67.85 kJ/m ³)	13.07	11.8
80/20 MGro Blend 11% Proctor (67.85 kJ/m ³)	11.20	31.9

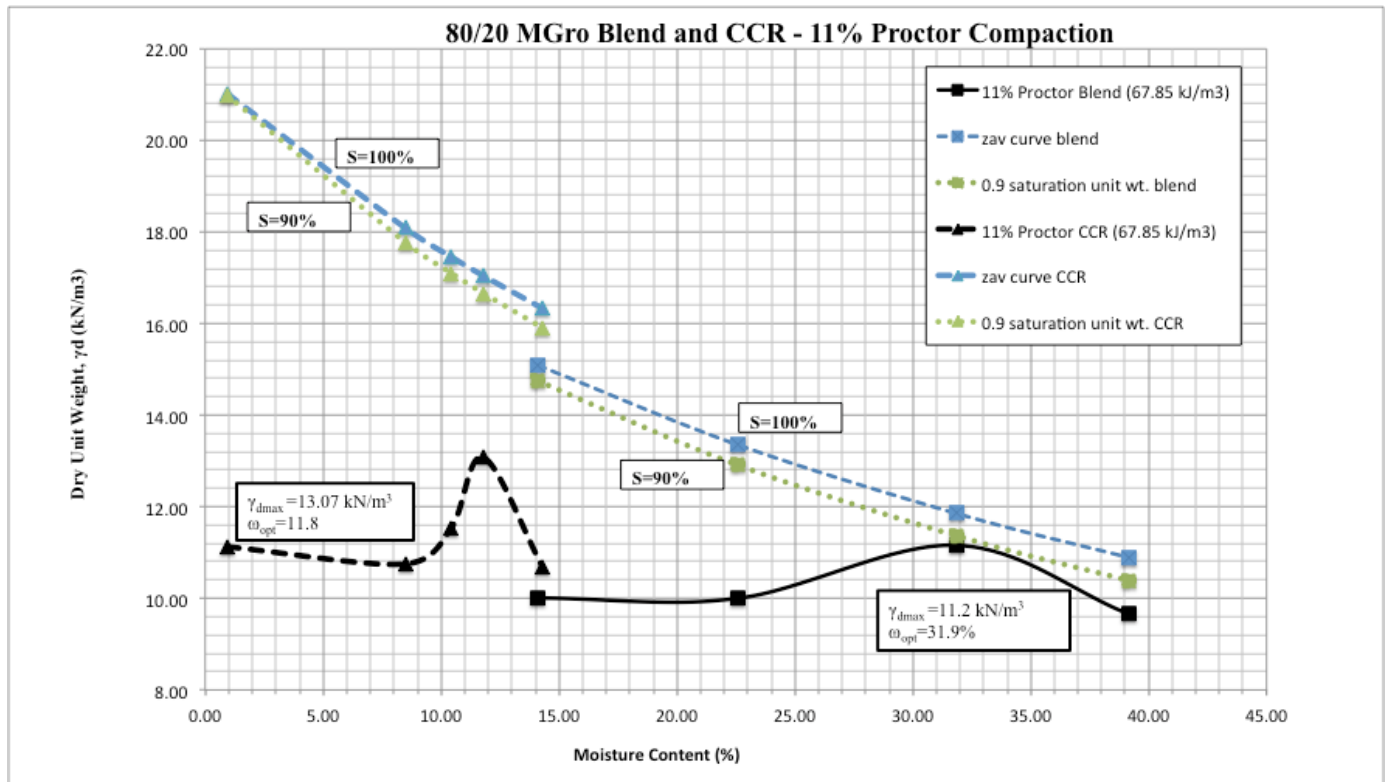


Figure 6. Compilation of compaction test results

The CCR curve at 11% Proctor shows that at low moisture content the material loses a small amount of density until it reaches 8.5%. From that point, it increases its density until reaching an optimum density of 13.07 kN/m³ at 11.8 % moisture. The blended material is at a much higher moisture content than the CCR. This can be attributed to MGroTM ability absorb large volumes of water. The curve starts at 15% moisture and maintains a constant density until 22.5% moisture. From that point the density increases gradually as moisture content also increases. The blended material reaches an optimum density of 11.2 kN/m³ at 31.9% moisture content.

There is a 1.87 kN/m³ decrease in density from the CCR test to the blended material. This can be attributed to the MGroTM material retaining more water, and creating an almost sludge-like finished product at much higher moisture content. The CCR is able to take in the water better and is much drier at its optimum density as can be seen in Figure 6.

Hydraulic Conductivity Testing Standard Proctor CCR Tests (592.5 kJ/m³)

Three tests were prepared at standard Proctor compaction (592.5 kJ/m³). These tests were targeted to reach a density of 15.9 kN/m³ and water content of 14.3%. The data and corresponding hydraulic conductivity can be seen in Table 7 below. These tests ranged from 10⁻⁶ to 10⁻⁷ cm/s that is common for coarse coal refuse. The test also proved to be accurate on the last five measurements as they show a coefficient of variation within 10%.

Table 7. Hydraulic Conductivity testing results for standard compacted CCR (592.5 kJ/m³)

Test	Water Content (%)	Dry Unit Weight (kN/m ³)	Degree of Saturation (S)	Porosity (n)	Hydraulic Conductivity Average (Last 5 Points) (cm/s)	Coefficient of Variation (Last 5 points) (cm/s)
1	14.21	15.7	84%	0.27	3.83 x 10 ⁻⁷	0.0980
2	15.01	13.9	61%	0.35	1.15 x 10 ⁻⁶	0.0783
3	15.51	13.9	63%	0.35	7.24 x 10 ⁻⁷	0.0454

The hydraulic conductivity of the specimens is plotted against the pore volume. Pore volume is defined as the porosity multiplied by the total specimen volume. The plot can be seen in Figure 7. A minimum of 1 pore volume was required to go through the specimen to ensure that full saturation had occurred, and a stable filter condition was achieved. Test 1 shows a large gap between 0 and 0.52 pore volumes. This is because a reading was not taken between 0 and 75 mL of water from the test. As can be seen in Figure 7, the test achieved a steady state with little variation in the data points. Test 2 had some fluctuations for the first 6 points, but quickly reach a steady state as it reached one pore volume. Test 3 had little fluctuation in the data, and quickly reached a steady state with almost no change in data points after 0.40 pore volumes. Test 1 tended to be slightly slower than tests 2 and 3 as can be seen in the plot. This is a direct cause to the dry unit wet being on the wetter side of optimum as indicated by the dry unit weight, and moisture content in Table 7.

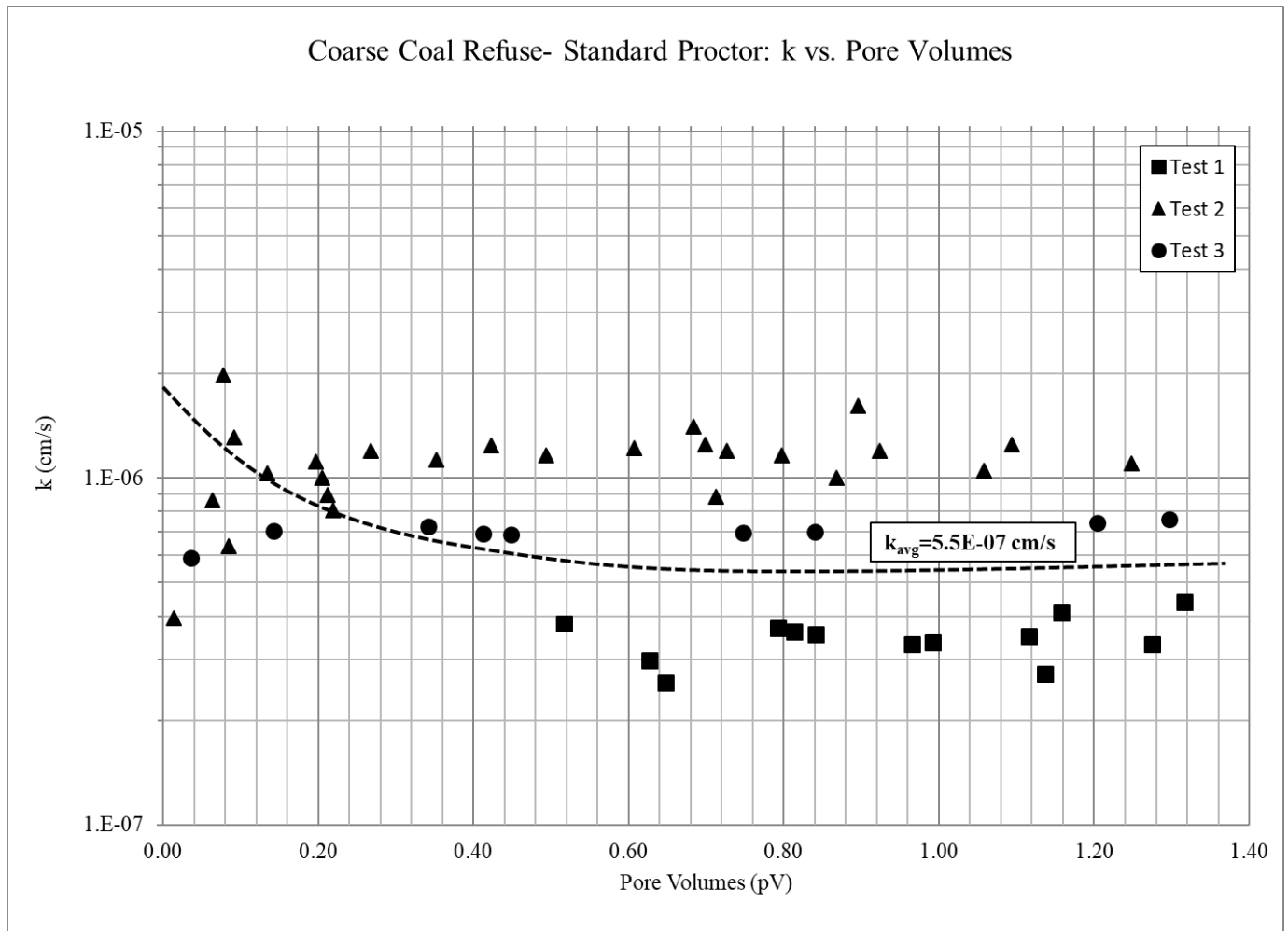


Figure 7. Hydraulic conductivity vs. pore volume plot for standard compacted CCR (592.5 kJ/m³)

11% Proctor 80%/20% CCR/MGro™ Growth Blend (67.85 kJ/m³)

Three tests were prepared at 11% Proctor for hydraulic conductivity testing. The specimens were made up of 80% CCR and 20% MGro™ for growth. The tests were targeted to reach a density of 11.2 kN/m³ at 31.9% moisture content. The data for the testing can be seen in Table 8 below. The hydraulic conductivity was in the magnitude of 10⁻⁴ cm/s which is fast, but the blend is supposed to allow water to permeate to ensure plant growth. The water contents did not meet the specific 31.9% moisture content range. This is due to the MGro™ material which has an ability to maintain a large volume of water and leads to large standard deviation of water content for each 80/20 blend. Sometimes a large amount of MGro™ could be in a moisture tin, or a small amount. Large amounts of MGro™ naturally leads to high moisture contents, while small amounts lead to low moisture content. The specimens still reach the target density or within 0.5 kN/m³.

Table 8. Hydraulic Conductivity results for 11% Proctor 80%/20% CCR/MGroTM blend (67.85 kJ/m³)

Test	Water Content (%)	Dry Unit Weight (kN/m³)	Degree of Saturation (S)	Porosity (n)	Hydraulic Conductivity Average (Last 5 Points) (cm/s)	Coefficient of Variation (Last 5 points) (cm/s)
1	21.83	11.7	57%	0.40	5.98 x 10 ⁻⁴	0.8913
2	19.18	11.2	69%	0.43	4.05 x 10 ⁻⁴	0.2938
3	25.55	11.5	62%	0.41	1.12 x 10 ⁻⁴	1.1830

The hydraulic conductivity is plotted against the pore volume for the three tests as well. It was maintained that the specimens reach at least one pore volume to reach a stable filter condition. The plot can be seen in Figure 8. The plot shows that all tests were run over more than one pore volume. This is due to the MGroTM material again. As mentioned, it holds in large volumes of water and has an ability to absorb water under a free swell condition, which can lead to large fluctuations in the permeability of the specimens. The plot shows more variability than the standard compacted tests shown in Figure 7. The coefficient of variation is also much higher as compared to the standard compacted specimens. This was expected with a material that takes in large amounts of water. The hydraulic conductivity for the three tests all are close in magnitude as shown in Table 8, in which all are in the order of 10⁻⁴ cm/s. It is believed that the tests reached stable filter conditions even with very high coefficient of variation for each test.

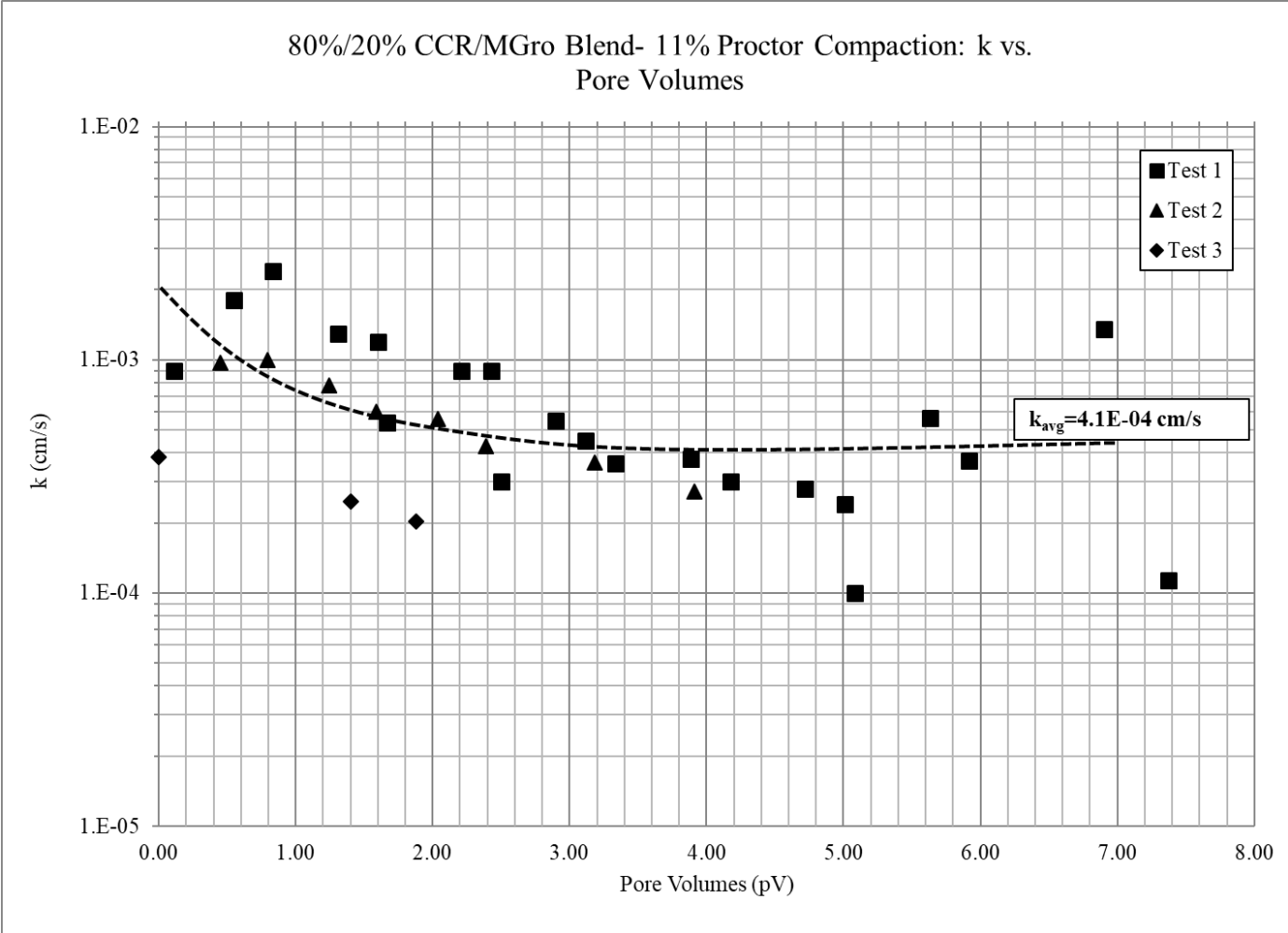


Figure 8. Hydraulic conductivity vs. pore volumes for 11% compacted 80%/20% CCR/MGroTM blend (67.85 kJ/m³)

Triaxial Compression Strength Testing Standard Compacted CCR (592.5 kJ/m³)-Total Stress Analysis

To determine when the material failed, the p - q plot must be analyzed according to a total stress analysis. The p - q plot can be seen in Figure 9. Failure on a p - q plot occurs when the curve changes from left to right at the large bend in each data series. This means when the bow in the curve changes from negative to positive. This large bend is the peak in stress difference for each curve. This can be specified on each plot by the white and black stars for each curve (CCR 1 through 4). Using the data from specified points where the stars are located, the strain rate at which the material fails can be defined in the stress-strain plot in Figure 10.

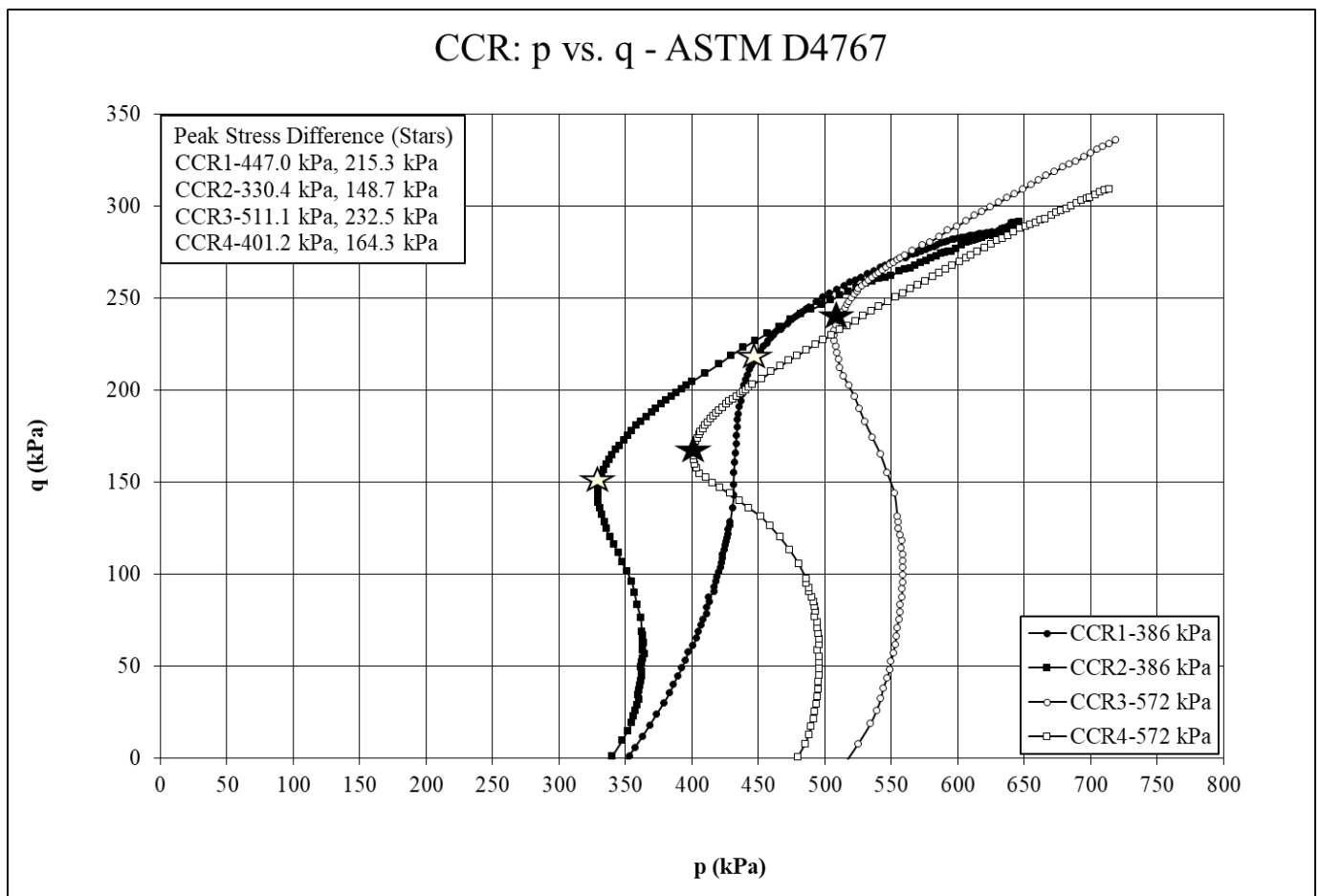


Figure 9. p - q plot for standard compacted CCR (592.5 kJ/m³)

Upon inspection of Figure 10, it can be inferred that there is no residual strength in each of the data series at different confining stresses. Each curve starts with some linear behavior before becoming curvilinear and continuing until around 20% strain. Without having a peak and a large reduction in shear stress that is prevalent in most stress-strain plots, the p - q plots were vital to determine at what percent strain the material failed at as mentioned in the above paragraph.

Using the corresponding stress where the stars are placed, the strain rate could be found by matching it to the stress-strain curve seen in Figure 10. The failure points are marked by white and black stars on the stress-strain plot.

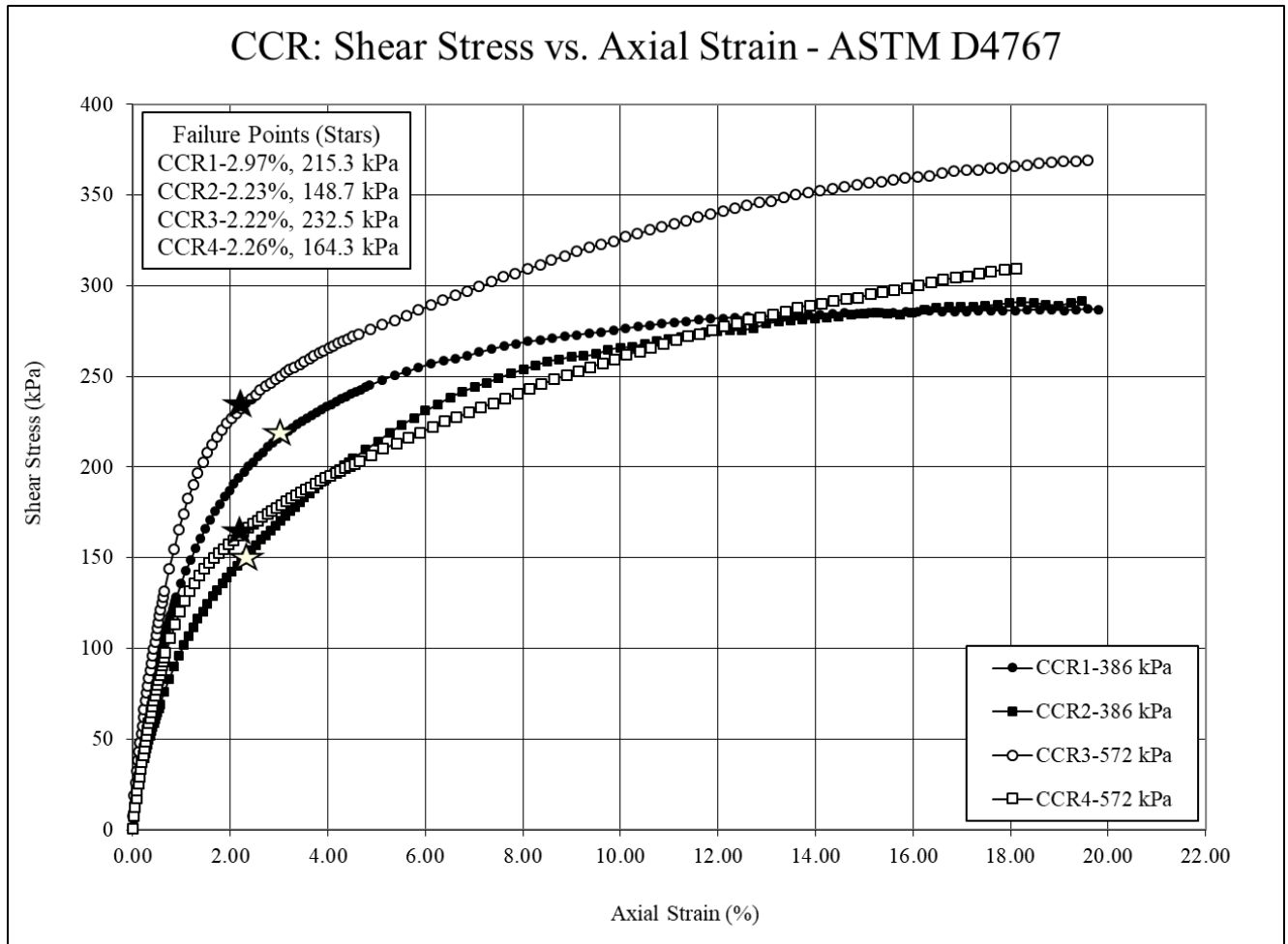


Figure 10. Stress-Strain plot for standard compacted CCR (592.5 kJ/m³)

As can be seen in the plot, the four materials failed between 2.22% to 2.97% strain. This shows that the materials had similar behavior at the two different confining pressures. To calculate the internal angle of friction, the maximum p and q values for each curve were analyzed. Due to assuming zero cohesion, equations 5 and 6 can be used to get an individual friction angle for each curve. Equations 5 and 6 are taken from the USACE Manual No. 1110-2-1902 (2003).

$$\alpha = \tan^{-1} \frac{q_{max}}{p_{max}}$$

(Equation 5)

$$\phi = \sin^{-1}(\alpha)$$

(Equation 6)

Table 9. Consolidated Undrained friction angle results for standard compacted CCR (592.5 kJ/m³)

Tests	Internal Angle of Friction (degrees)
CCR1-386 kPa	24.89
CCR2-386 kPa	25.08
CCR3-572 kPa	24.78
CCR4-572 kPa	24.12

Table 10. Summary statistics for friction angle results (standard compacted CCR) (592.5 kJ/m³)

Summary Statistics for Standard Compacted CCR	
Average	24.72
Standard Deviation	0.417
Coefficient of Variation	0.0169

The results in Tables 9 and 10 shows that the results from the CU were accurate and ranged from 24.12-25.08 degrees with an average of 24.72 degrees. The coefficient of variation for these results are low for a small sample size. The average is close to a 2:1 slope (26.6 degrees), which is good in terms of stability.

11% Compacted 80/20 CCR/MGro™ blend-Total Stress Analysis

A total stress analysis was also done on the 80/20 replicants to gain friction angle and determine where failure occurred. *P-q* plots were generated for analysis, but the results in Figure 11 do not exhibit the curvilinear negative to positive that determined failure for the standard compacted CCR. 80/20-1 shows that the path presented horizontal behavior going back and forth. 80/20-2 had very low values on the q-axis, and had large skewed data fluctuations. 80/20-3 presented completely linear behavior from 0-21.2 kPa on the q-axis, and 50.6-90.1 kPa on the p-axis. 80/20-4 showed some linear behavior before reversing its trend in the opposite direction. The reversing means that the material goes into compression or failure.

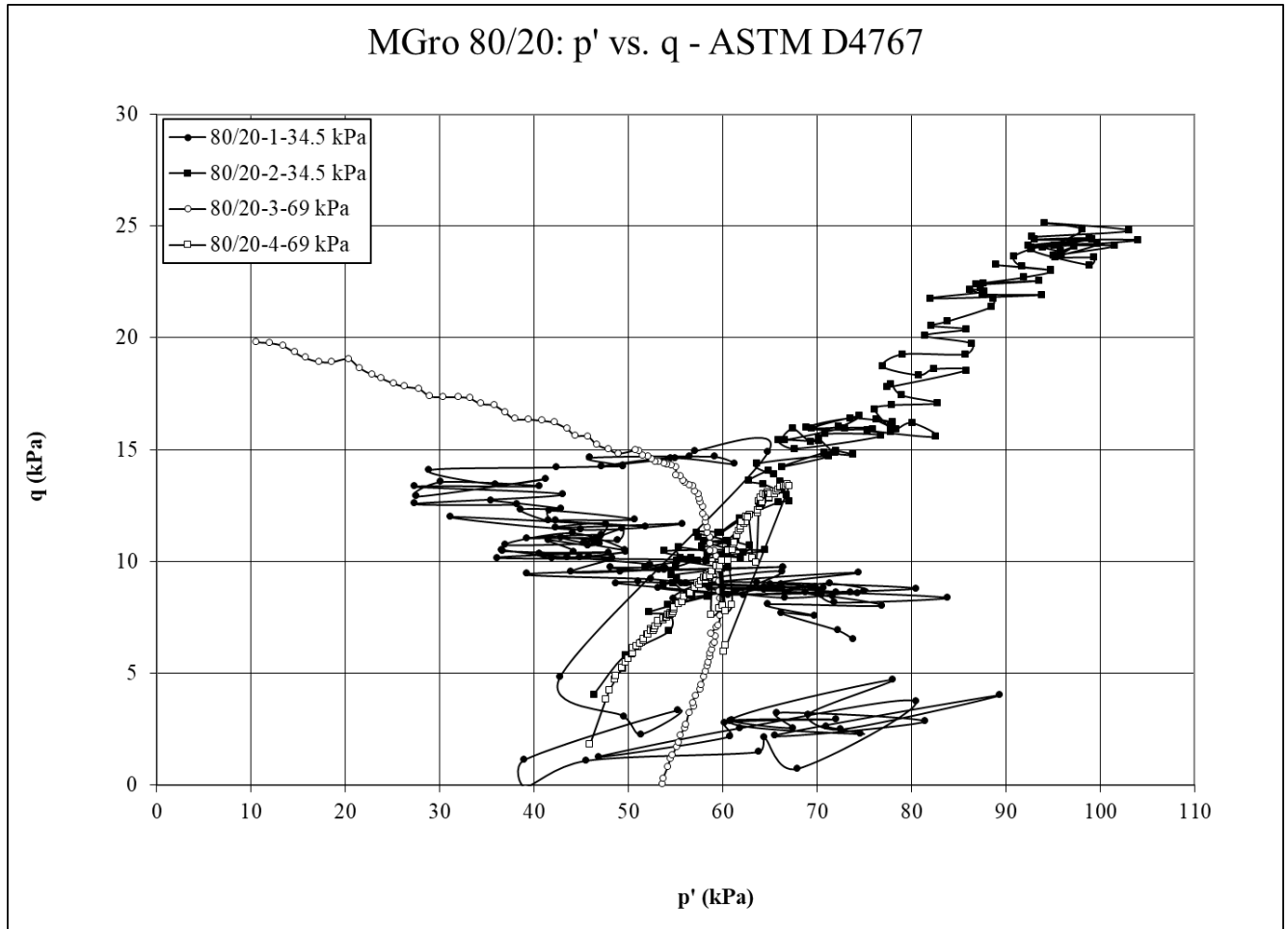


Figure 11. *p-q* plot for 11% compacted 80/20 CCR/MGroTM blends (67.85 kJ/m³)

The reason for the behavior can be attributed to the very low compaction effort that was applied to the specimens, and the way MGroTM behaves naturally. With constant cell-pressure the axial piston applies a compressive stress to the specimen. With a light compaction effort, and MGroTM making up 20% of the specimen; the specimen went under a compression behavior like a sponge due to the large amounts of water present in MGroTM. This could cause the specimens to deform rapidly and give data that is present in Figure 11.

To identify when the material failed, a different approach was taken. The *p-q* plots show a back and forth behavior, which means the specimens failed at a very low strain. To see how low of a strain, the Mohr-Coulomb stress-strain plot was analyzed, since failure cannot be determined from the *p-q* plots. Referring to Figure 12, the materials show little to no residual strength. This is a verification of a constant strain failure. Upon inspection of Figure 12, the failure points can be verified. 80/20-1 and 80/20-2 fails at less than 1% strain. Both replications start an increase and decreasing trend early in their respective curves. This increase/decrease is indicative of failure, and both continue with constant strain to 20% except for 80/20-2 having a 10 kPa

decrease in stress. These blends are also the lower of the two confining pressures. 80/20-3 and 80/20-4 fails at less than 4% strain at a higher confining pressure. Blend 3 fails early in the test by a small decrease in stress, while 80/20-4 has a 1.95 kPa decrease in stress indicating failure. 80/20-4 continues the decreasing trend before continuing constant strain through 20%.

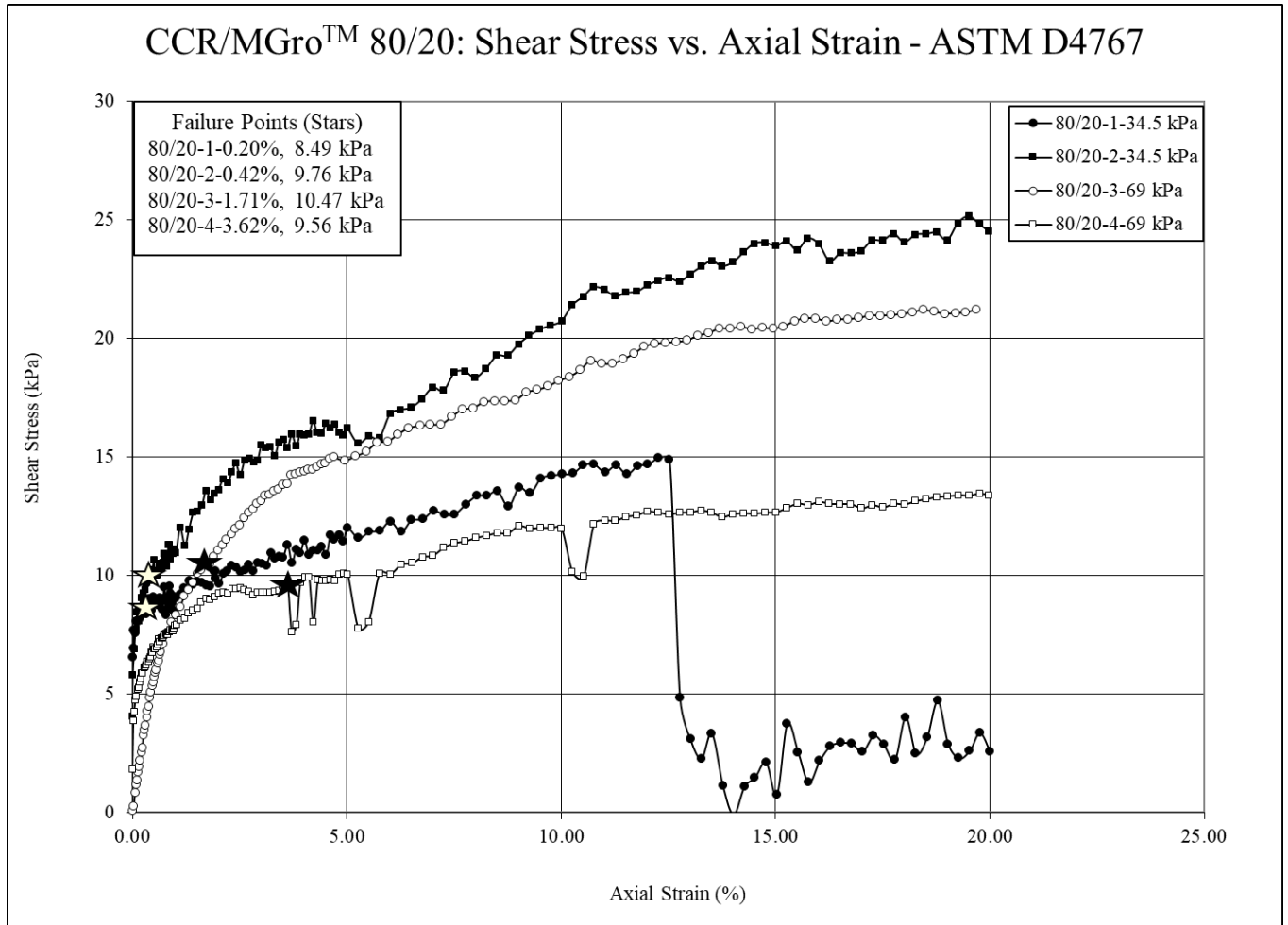


Figure 12. Stress-Strain plot for 11% Compacted 80%/20% CCR/MGro™ blend (67.85 kJ/m³)

Figure 12 indicates that the blends reached peak strength (failed) and continued constant strain behavior. The plots have some similarities in behaviors besides the large decreases in stress for each confining pressure. These large drops can be attributed to the low compaction effort, and MGro™ material as the axial load was applied. The next step was to calculate the internal angle of friction for the blend material. Equations 5 and 6 were used to calculate the internal angle of friction using the maximum p and q values gained from testing. The assumption of zero cohesion was also applied for this sweep of testing similar to the standard compacted CCR.

Table 11. Consolidated Undrained friction angle results for 11% Compacted 80%/20% CCR/MGroTM blends (67.85 kJ/m³)

Tests	Internal Angle of Friction (degrees) (degrees)
Blend1-34.5 kPa	10.60
Blend2-34.5 kPa	16.67
Blend3-69.0 kPa	13.37
Blend4-69.0 kPa	12.30

Table 12. Summary statistics for friction angle results (11% Compacted 80%/20% CCR/MGroTM blends) (67.85 kJ/m³)

Summary Statistics for 11% Compacted 80/20 Replications	
Average	13.24
Standard Deviation	2.558
Coefficient of Variation	0.1933

Tables 11 and 12 shows that the friction angles ranged from 10.60-16.67 degrees with an average of 13.24. This is wide range for friction angles, but this is expected from a material that has very low density. This material will also serve as the top layer (cover) and is only one foot in thickness. This very low friction angle can also be explained by MGroTM. MGroTM is highly organic, and materials that have a high organic content can produce very low internal angles of friction in the range of 0-10 degrees (Koloski et al. 1989). The results for this testing did not fall in that range, but can serve as a guideline for the low internal angles of friction. The coefficient of variation for the blend testing is also high which is expected with a large range of friction angles.

11% Compacted 80/20 CCR/MGroTM blend-Effective Stress Analysis

An effective stress analysis was also done on an 80/20 replication to see the differences between a total and effective stress path. The confining pressure for this test was at 69 kPa similar to the total stress analysis. The major difference in the effective stress analysis is that it takes into the consideration the subtraction of pore-water pressure from the major and minor principal stresses. Instead a p - q plot, a p' - q' plot will be used to analyze for failure and friction angle. The p' - q' plot can be seen in Figure 13.

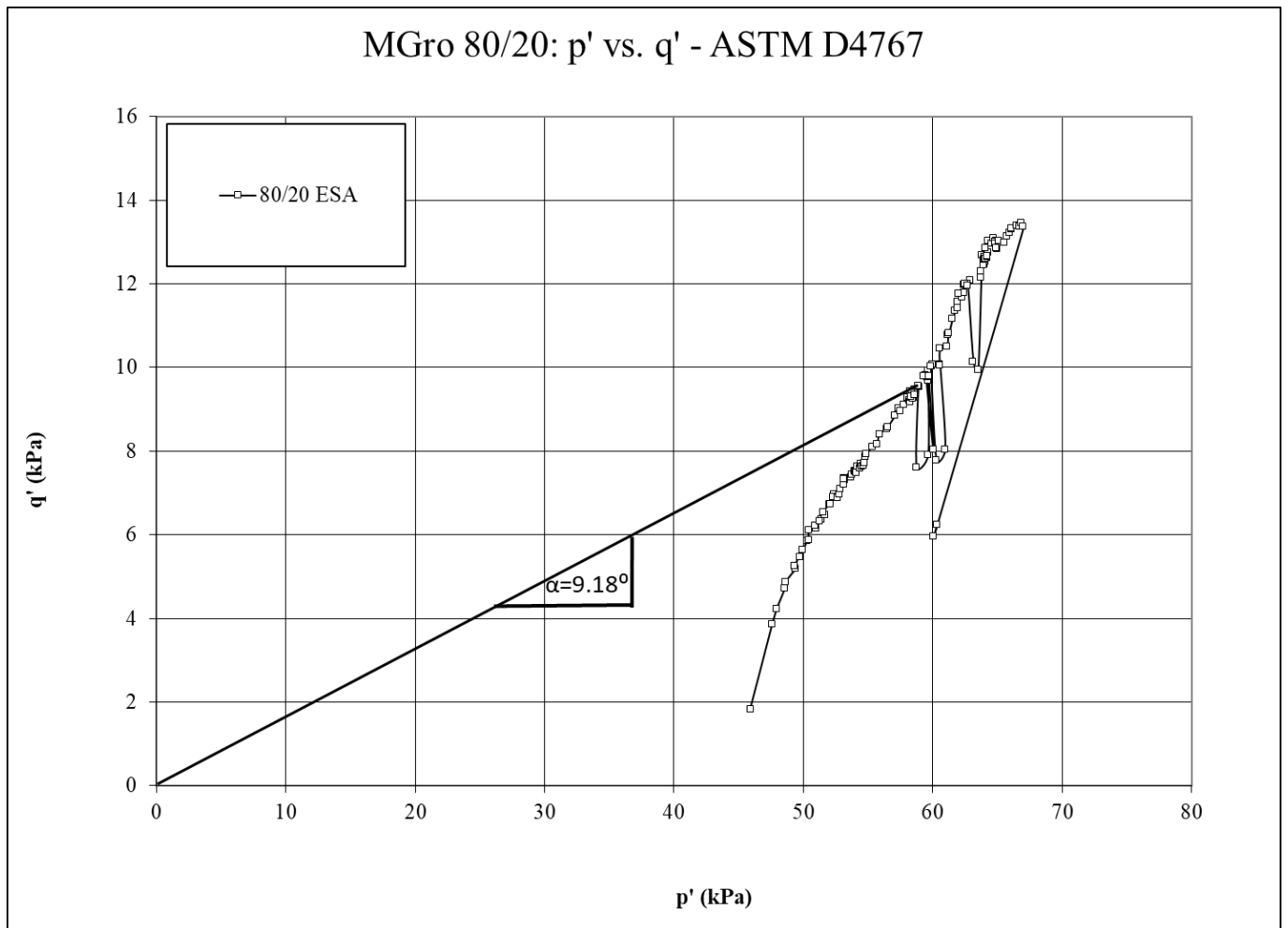


Figure 13. p' - q' plot for 11% compacted 80/20 CCR/MGroTM blend (67.85 kJ/m³)

The p' - q' plot shows a much different curve than what was seen in Figure 11. The curve shows that as stress increases up to its failure point at (58.95 kPa, 9.54 kPa). After that there is a 1.93 decrease in stress at the first large drop. A line of best fit was also used to gain the alpha angle for this set of data. The test was under the assumption of zero cohesion as the line is drawn through the (0,0) axis. The alpha angle was found to 9.18 degrees, and from that point the friction angle could be calculated. Equation 7 shows the calculation of the friction angle based off the alpha angle of the best fit line and was taken from the USACE Manual No. 1110-2-1902 (2003).

$$\phi = \arcsin(\tan(\alpha))$$

Equation 7

Table 13. Consolidated Undrained friction angle results for 11% compacted 80/20 blend (67.85 kJ/m³)

Tests	Internal Angle of Friction (degrees)
80/20 Blend-69.0 kPa	9.30

The friction angle according to the effective stress analysis was 9.30 degrees as seen in Table 13. This is lower than the four friction angle results from the total stress analysis. The lowest friction angle for the total stress analysis was 10.60 and the highest 16.67. The decrease in friction angle from the effective stress analysis is accredited to the pore-water pressure being subtracted from major and minor principal stresses in the stress-path plot (Figure 13). A pore-pressure-strain plot can be seen in Figure 14 as well. The plot shows that the 80/20 blend went under dilation or an extension of the sample. Most samples when the axial piston is applied go under compression. The extension of the blend is due to the MGro™ in the sample is water retentive when it is compressed. It is also noted that first large decrease in in pore-water pressure is at 3.62% strain, which is what was considered failure for the total stress analysis.

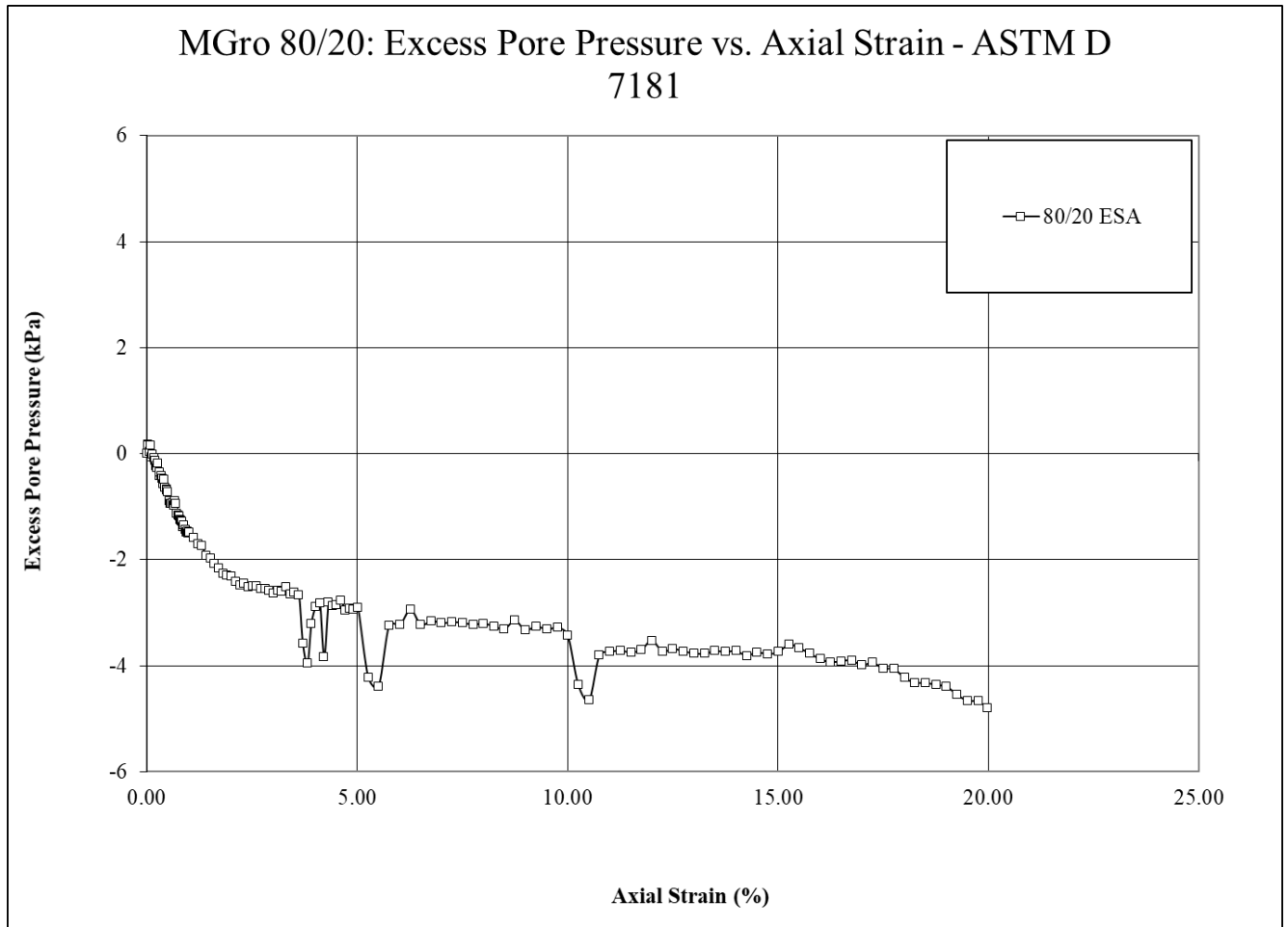


Figure 14. Pore-water pressure versus axial strain for 11% compacted 80/20 CCR/MGroTM blend (67.85 kJ/m³)

Summary of Geotechnical Laboratory Testing Results

Table 14 tabulates the results of geotechnical laboratory testing performed for the Royal Scot site. The research for this study focused on a larger gradation size for CCR, and 80/20 blend testing. A previous researcher did CCR testing and 60/40 blend testing using the same material from their respective sites (Stevens, 2016). There are numerous similarities and differences between this study and the previous researcher’s studies that will be discussed in detail.

A full sweep of geotechnical testing was done on the standard compacted CCR (592.5 kJ/m³) and 11% compacted 80/20 CCR/MGroTM blends. Grain size distribution was performed on CCR passing a 19-mm sieve (3/4”), and then compaction, hydraulic conductivity, and triaxial strength testing was performed on the standard compacted CCR, and 11% compacted blend materials. Research by Stevens (2016) on materials similar to the standard compacted CCR, 11% compacted blend material, and used a 60/40 CCR/MGro blend. The CCR and MGroTM materials were taken from the same sites. Table 14 summarizes the material properties tested in this research and lists the corresponding data from Stevens (2016).

Table 14. Parameter summary table for Geotechnical lab testing

Royal Scot Laboratory Parameter Summary Table					
Geotechnical Property	CCR Shale (Stevens, 2016)	MGro™ (Stevens, 2016)	60/40 CCR- MGro™ blend (Stevens, 2016)	80/20 CCR/MGro™ blend	CCR Passing 19 mm
D ₁₀ Sand Portion (#4 - #200) (mm)	0.53	0.98	0.3	0.3	0.3
D ₅₀ Sand Portion (#4 - #200) (mm)	1.72	3.35	1.7	1.6	3.0
% Passing No. 200 sieve (clays and silts)	1.23	0.42	2.96	2.75	3.62
Specific Gravity G _s	2.19	1.92 - 2.21	-	-	-
Plasticity Index, PI	4	-	-	-	-
k _{sat} (cm/s)	3.50E-07 - 4.22E-04	-	8.61E-04	3.34E-04	6.87E-07
φ' (degrees) Direct Shear	41.40 - 43.80	-	30.16	-	-
φ' c'=0 (degrees) Direct Shear	43.21 - 44.96	-	35.82	-	-
c' (kPa)	16.99 - 25.60	-	1.92	-	-
φ' c'=0 (degrees) ICU	-	-	-	9.30-16.77	24.12-25.08
γ _{dmax} (kN/m ³) (200% Proctor)	16	-	-	-	-
γ _d (lb/ft ³) (200% Proctor)	101.9	-	-	-	-
ω _{opt} (%) (200% Proctor)	12.3	-	-	-	-
γ _{dmax} (kN/m ³) (Standard Proctor)	15.9	-	-	-	-
γ _d (lb/ft ³) (Standard Proctor)	88.3	50.9	74.5	-	-
ω _{opt} (%) (Standard Proctor)	14.3	-	-	-	-
γ _{90%} (lb/ft ³)	87.57	-	74.08	-	-
ω _{90%}	12.8	-	27.2	-	-
γ _{dmax} (kN/m ³) (34% Proctor)	15.1	-	-	-	-
ω _{opt} (%) (34% Proctor)	17	-	-	-	-
γ _{dmax} (kN/m ³) (11% Proctor)	14.6	-	11.7	11.2	13.07
ω _{opt} (%) (11% Proctor)	17.5	-	28	31.9	11.8

* Dashes (-) represent lab testing that is not available. *

Observations of CCR geotechnical laboratory testing:

For the GSD testing, there are some differences with the indices listed in Table 14. As mentioned a larger gradation was used for this study, and was sieved in the field up to 19 mm. Stevens (2016) shows that there are larger diameter particles at the sand portions of D₅₀ and D₁₀. The reason for this is that the testing done for this report was already sieved in the field and put through the GSD procedure. The testing done by Stevens (2016) used *in-situ* material, which had very large (50.8 mm) material that sat on top of the #4 sieve. That is the reason for the smaller values of 1.72 and 0.53 mm for D₅₀ and D₁₀, as opposed to 3.0 and 0.30 mm.

The combined GSD can be seen in Figure 5. The percent passing a No. 200 sieve for this study produces more crushed fines in the silt and clay range particles (fines) as opposed to Stevens as well, which is expected with smaller diameter particles (Stevens, 2016). The final comparison for the GSD is that the material for this study classifies as a well graded sand with gravels (SW) as opposed to Stevens' poorly graded sand with gravels (SP). This is due to (Stevens, 2016) having a large (50.8 mm) shale material that is mentioned above. That large piece of shale changed the coefficient of uniformity, which governs the final classification from well to poorly graded.

Compaction testing was performed on two 11% Proctor energies, which consisted of CCR, and an 80/20 blend. The 11% compaction (67.85 kJ/m^3) was used to approximate the refuse at a density approximate to being end-dumped from a loader or similar construction equipment. In comparison, Stevens (2016) had two 11% compaction specimens, which were CCR and a 60/40 blend. A major difference for the CCR was that for this study, a max 19 mm gradation was used and Stevens used a max gradation of 4.76 mm (#4 sieve), which is four times as large. Table 14 shows that the dry unit weight and moisture content for the larger gradation decreased by 1.53 kN/m^3 and 5.7% respectively. For a shale material, the larger the particle size, the less water it can hold in, which is in accordance with the results from the laboratory testing. The 80/20 and 60/40 blends show that they both performed very similarly. 80/20 blend had a dry unit weight and moisture content of 11.20 kN/m^3 and 31.90%, while 60/40 had 11.70 kN/m^3 and 28.00%. Both are very close in density and moisture content, with 60/40 having a 0.5 kN/m^3 increase in density with a lower moisture content. This can be explained for either material by inconsistencies with the MGro™ material. Any moisture content that is taken to be dried during compaction testing could have a large amount or small amount of MGro™. The more MGro™; the higher moisture content, and vice-versa.

For the hydraulic conductivity testing, standard compacted CCR (592.5 kJ/m^3) and 11% compacted 80/20 blend (67.85 kJ/m^3) testing will be compared to Stevens testing (Stevens, 2016). Both tested standard compacted CCR, but the research done for this study was done with flexible-wall testing as opposed to rigid-wall testing. Flex-wall was chosen because of the possibility of particle migration in rigid-wall permeability testing. Under standard compacted conditions for CCR, both studies show that the laboratory permeability of two different max gradation had velocities in the magnitude of 10^{-7} cm/s . For this research, it was expected that the larger 19 mm gradation, would have a much faster permeability, but that was not the case as both performed similar according to Table 14. This study had a hydraulic conductivity of $6.87 \times 10^{-7} \text{ cm/s}$, which Stevens posted $3.50 \times 10^{-7} \text{ cm/s}$. The 80/20 and 60/40 CCR/MGro™ blends had much lower magnitudes but similar conductivities once again. Both blends were in the magnitude of 10^{-4} cm/s . The expectation for the 80/20 blend was that it would be in the order of 10^{-3} cm/s with a 50% reduction of MGro™, but that was not the case. MGro™ takes in large amounts of water so it was expected to be able to flow faster through a larger 19 mm max gradation than with 50% more MGro™ and a smaller 4.76 mm max gradation.

The final testing comparison is for the internal angle of friction for standard compacted CCR, and 11% blends that were tested. First, this study used isotropic triaxial compression ICU testing, while Stevens (2016) used direct shear testing. Reference to Table 14, presents the friction angles under cohesionless conditions show the friction angle results are much higher than the results of the ICU testing. The standard Proctor compacted CCR posted friction angles ranging from 24.12-25.08 degrees, while Stevens (2016) results were 43.21-44.96 degrees. The 80/20 testing had a range of 9.30-16.77, while 60/40 was 35.82 degrees. The lower bound (9.30 degrees) was analyzed using an effective stress analysis, while the upper bounds were calculated using a total stress analysis. This is a very large difference between two similar materials. As mentioned, the maximum gradation size for this study was four times as large as the gradation for Stevens, and there was a 50% reduction of MGroTM between 60/40 to 80/20. This does not mean that the gradation/reduction is the direct cause. The main cause for this result is likely due to the change of testing procedure and the behavior of the refuse under the ICU conditions. Typically for direct shear, materials with very small particle size are used. The GSD (Figure 5) results for passing a #200 sieve in Table 14 show that very little clay/silts were present in the materials (less than 5%). During the direct shear test, a larger particle could have been at the threshold of the shear plane. The particles shape and orientation then could force the material to have higher friction angles than expected.

Numerical Modeling

To see the effects of the laboratory testing on the Royal Scot site, Finite Element Modeling (FEM) was performed on two separate 2D slopes. The first slope was a conventional planar slope that had geometry close to a 2:1 profile. The other slope was a geomorphic channel. These two slopes performances will be measured using seepage and slope stability analysis. An image of the Royal Scot site with the locations of these slope profiles can be seen in Figure 15. The locations are indicated by the black boxes. The conventional planar slope located near Ditch G includes one bench that measures 7 feet. The geomorphic slope does not have benches and is less steep.

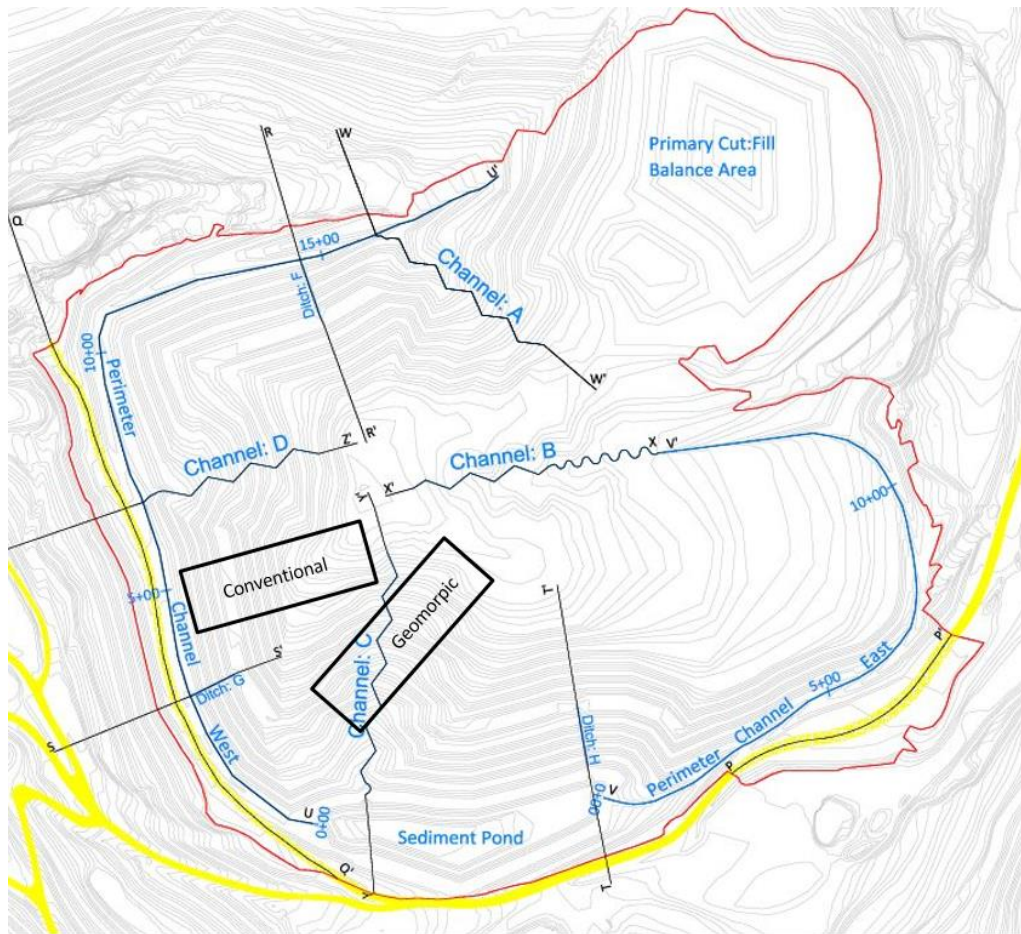


Figure 15. Image of Royal Scot plan including the location of slope profiles that are modeled (Adapted from Lorimer, 2016)

Modeling Methodology

The modeling for this study was done using SVOOffice™. Within SVOOffice™ there are two programs named SVFlux™ and SVSlope®. SVFlux™ was used for the seepage analysis implementing climate into the two slope profiles. SVSlope® was used for slope stability analysis after the seepage analysis has occurred. This allows the slope to be analyzed for stability after the soil has become saturated, simulating a worst-case scenario. These two programs allowed the

overall performance of the cap and cover system to be evaluated at according to the laboratory testing. The models were also analyzed using unsaturated soil mechanics. This means that the all soil profiles were modeled as an unsaturated condition, until the a 100-year storm occurred.

SVFlux™

The two slope profiles were run for 25 days within SVFlux™. The 25 days is to see how a 100-year 24-hour storm infiltration affects the Royal Scot site. The storm was inserted on the first day of the model, and seepage affects were analyzed. The data was gathered from the NOAA Point Precipitation Frequency Estimates. Table 15 list all the details of the storm event.

Table 15. Probabilistic storm data for modeling

Storm Event	Station	Volume (m/day)
100-year 24-hour	East Rainelle 3 NNE	0.135

The station used was close to the Royal Scot Site and was East Rainelle 3 NNE (46-2638) station. The 100-year storm had a volume of 0.135 m/day. This storm should allow the growth (cover) layer to completely saturate and see how much water infiltrates into the hydraulic barrier. The storm data could be input into the SVFlux™ via climate boundary condition. The other boundary condition that was used in SVFlux™ consisted of review boundaries. A review boundary is used in SVFlux™ to allow flow into or out of the model depending on differences in pressure. These were used on both models to allow the fluxes to flow into or out of the model. The last condition that was inserted into the model were flux lines. Flux lines are used to track the amount of flux that travels through the line. The flux lines in this model were used to track infiltration from the hydraulic barrier into the fill material. The flux line was drawn from the bench of the conventional planar slope to the toe under the hydraulic barrier layer. The flux line reports infiltration in cubic meters of flow. Since it is a 2-D model, the thickness of the slope is 1-meter so that cubic meters of infiltration is possible. For the geomorphic slope, the line was drawn from lower 66% of the slope to the toe under the hydraulic barrier. Table 16 shows a list of boundary conditions and their location on the two slope profiles.

Table 16. Boundary condition locations

Boundary Conditions	Locations
Climate Boundary	Top of growth layer
Review Boundary	Toe of slopes
Flux Line (Conventional)	Bench to toe
Flux Line (Geomorphic)	Lower 66% to toe

SVSlope®

SVSlope® is the finite element analysis program used for the analysis of slope stability based on the limit equilibrium approach. For this study, the slopes will be analyzed in two dimensions. The program includes several material failure modes including Mohr Coulomb, Hoek-Brown, and several others; for this analysis Mohr-Coulomb will be used. SVSlope® also has several calculation methods for safety factors. Some of these methods include: General Limit Equilibrium (GLE), Bishop's simplified method of slices, Janbu method of slices, and several others. For this analysis, the GLE was chosen because it takes into consideration the inter-slice shear forces. Another useful tool within SVSlope® is the ability to couple with SVFlux™ for transient analysis with saturation and groundwater data. Coupling the two programs allows the user to see the effects of pore-water pressure and climate on the slope profiles.

Unsaturated Soil Mechanics

The growth layer will be saturated during a storm event, so the cap part of the system will be modeled as a saturated condition. This will not be the case for the hydraulic barrier and the fill material. The barrier and fill material will be modeled as an unsaturated condition. The barrier is designed to saturate over time due to storms, and allow little to no water to seep into the fill material.

Therefore, unsaturated hydraulic conductivity calculations were required for these cover systems. The unsaturated soil properties were done using the Fredlund and Xing equation for the Soil-Water Characteristic Curve (SWCC) (Lu and Likos 2004). The equation can be seen below in Equation 8.

$$\theta(\psi) = \left(1 - \frac{\ln\left(1 + \frac{\psi}{\psi_r}\right)}{\ln\left(1 + \frac{10000000}{\psi_r}\right)}\right) \theta_s \left(\frac{1}{\left(\ln\left[e + \left(\frac{\psi}{a}\right)^n\right]\right)^m}\right) \quad (\text{Equation 8})$$

where,

θ = volumetric water content (%)

ψ = matric suction (kPa)

ψ_r = matric suction corresponding to residual water content = h_r (kPa)

θ_s = saturated volumetric water content (%)

a : curve fitting parameter

n : curve fitting parameter

m : curve fitting parameter

h_r : curve fitting parameter

There was one issue with the curve fitting parameters: a , n , m , and h_r . The parameters are based on D_{10} from the grain size distribution and gave results that were not justifiable. It was then discovered the Torres (2011) equation could be used for large coarse materials. The D_{10} of 0.28 mm from Table 4 was not able to fit the Torres' equations so a maximum value of D_{10} equal to 0.11 was used for the SWCC. The fitting parameters for the Torres Equation can be seen below.

$$a_f = -967.21(D_{10}^2) + 218.37(D_{10}) - 2.7 \quad \text{(Equation 9)}$$

$$n = 10^{(-0.0075a_f^3 + 0.1133a_f^2 - 0.3577a_f + 0.3061)} \quad \text{(Equation 10)}$$

$$m = 0.0058a_f^3 - 0.0933a_f^2 + 0.4069a_f + 0.3481 \quad \text{(Equation 11)}$$

$$h_r = 100 \quad \text{(Equation 12)}$$

Table 17. Soil Water Characteristic Curve (SWCC) Parameters

Soil Water Characteristic Curve	Parameter
a_f	9.62
n	4.72
m	0.79
h_r	100

Modeling Inputs

For SVFluxTM and SVSlope[®] to give accurate results, input parameters from geotechnical laboratory testing were used. For SVFluxTM properties include hydraulic conductivity, volumetric water content, and Soil-Water Characteristic Curve variables are used. SVSlope[®] uses failure mode parameters. Since Mohr-Coulomb is used for this analysis, input parameters include: dry unit weight, cohesion, and internal angle of friction.

SVFluxTM Input Parameters

The input parameters for SVFluxTM consist of saturated hydraulic conductivity and volumetric water content (porosity (n)), and specific gravity (G_s). Aside from these two parameters, the soil-water characteristic curve includes data that corrects the hydraulic conductivity for an unsaturated scenario. The data that was used are the Equations 9 through 12 (Torres, 2011). The equations are related to D_{10} of CCR shale. Figure 5 shows a compilation of the GSD curves. The original results for D_{10} (0.30 mm) of the CCR shale gave undesirable results for the fitting parameters. A D_{10} value of 0.11 mm was used as the maximum for the fitting parameters according to the Torres equation. The D_{10} particle size yielded fitting parameters of $a_f=9.62$, $n_f=4.72$, $m_f=0.79$, and $h_r=100$. Parameter a_f governs the approximate air entry value, n_f controls

the slope of the curve at its inflection point, m_f is related to the residual water content, and h_r correlates to matric suction under residual water conditions (DePriest, 2015). The input parameters for SVFluxTM are presented in Table 18.

Table 18. SVFluxTM input parameters for modeling

SVFluxTM Input Parameters			
Input Parameters	80/20 Blend	Hydraulic Barrier	Fill CCR
k_{sat} (m/day)	0.289	0.0594	0.3456
volumetric water content (n)	0.48	0.35	0.45
G_s	2.00	2.19	2.65

SVSlope® Input Parameters

As mentioned, dry unit weight, cohesion, and friction angle are the major input parameters for SVSlope®. The dry unit weight and cohesion stayed constant on both slope profiles, and were not changed. Dry unit weight takes the water content into consideration. For the internal angle of friction, a sensitivity analysis was performed according to the Three-Sigma rule for small sample sizes to account for uncertainty in the hydraulic barrier and 80/20 growth layer. According to Duncan (2000), the Three-Sigma Rule uses the fact that 99.73% of all values of a normally distributed parameter fall within three standard deviations of the average. The Three-Sigma rule can be used to estimate a value of standard deviation by first obtaining highest and lowest conceivable values of the parameter. Equation 13 shows the equation for the estimated standard deviation (Duncan, 200)

$$\sigma_3 = \frac{HCV-LCV}{6} \tag{Equation 13}$$

HCV=highest conceivable value

LCV=lowest conceivable value

Table 19. 3-Sigma friction angle values

Hydraulic Barrier	LCV	Mean	HCV
Friction Angle (degrees)	24.24	24.72	25.20
Standard Deviation (degrees)	0.16		
80/20 Growth Layer	LCV	Mean	HCV
Friction Angle (degrees)	10.22	13.22	16.22
Standard Deviation (degrees)	1.0		

Three friction angle values for the hydraulic barrier and 80/20 growth layer were chosen for the two slope profiles according to the sensitivity analysis. The values are listed in Table 19. The highest conceivable (HCV), mean, and lowest conceivable (LCV) values were all run in SVSlope® to establish a parametric range of safety factors. The rest of the input parameters are presented in Table 20. The commas for the friction angle values is the different angles that were chosen based off the Three-Sigma analysis, that were listed in Table 19. All parameters used for the slope stability analysis were laboratory tested apart from the inputs that have an asterisk (*) next to them. These were recommended to use for the fill material, since laboratory testing had not been done on that material (Stevens, 2016). The c' (cohesion) has very low values due to the inherent nature of the refuse. In the laboratory testing, zero-cohesion assumptions were used since the material was shale, and produces a small number of fines. The model is not able to run with zero inputted for cohesion, so very small values were used for each layer.

Table 20. SVSlope® input parameters for modeling

SVSlope® Input Parameters			
Input Parameters	80/20 Blend	Hydraulic Barrier	Fill CCR
ϕ (°)	10.22, 13.22, 16.22	24.24, 24.72, 25.20	40.54*
c' (kPa)	1.00	2.00	2.00
γ (kN/m ³)	11.20	15.90	18.02*

* signifies parameters done by Stevens, 2016

Modeling Results

Using the input parameters for SVFlux™ and SVSlope®, the conventional planar slope and geomorphic could be analyzed for seepage and stability. Both conventional and geomorphic slopes had a 0.6-meter (2 ft) hydraulic barrier and 0.3-meter (1 ft) 80/20 growth layer. The only difference was the conventional planar slope had a 0.6-meter barrier through the benched area, and was then tapered to 0.3 meters on the downslope toward the toe of the slope. This taper was to reduce pore pressure build-up that happens in conventional planar slopes toward the toe due to a saturated hydraulic barrier. For the hydrologic output, both slope profiles were analyzed for precipitation and infiltration from the hydraulic barrier into fill material. The growth layer is designed to experience a large amount of infiltration due to its light compaction effort. This also allows excess water to ensure plant growth.

The models simulated the effects of a 100-year 24-hour storm event (0.135 m/day or 135 mm of rainfall). The slopes were modeled to be in a partially saturated state, and the storm event occurred on day 1 of 25 successive days. The 25-day duration allows the movement of infiltration and saturation of the slope after a 100-year storm has occurred. Slope stability calculations were done after the storm event has occurred to get a worst-case scenario on the lowest factor of safety for the conventional planar and geomorphic slopes.

Conventional Planar Slope (Ditch G) Saturation and Streamlines

Figures 16 to 19 show the saturation of the conventional planar slope before and after the storm event. Table 21 helps to identify the saturation on each corresponding day.

Table 21. Saturation of growth layer and hydraulic barrier

Conventional Planar Ditch G		
Day	Growth Layer Saturation (%)	Hydraulic Barrier Saturation (%)
3	100	40 to 50
4	100	50
15	100	20 to 30
25	100	15 to 20

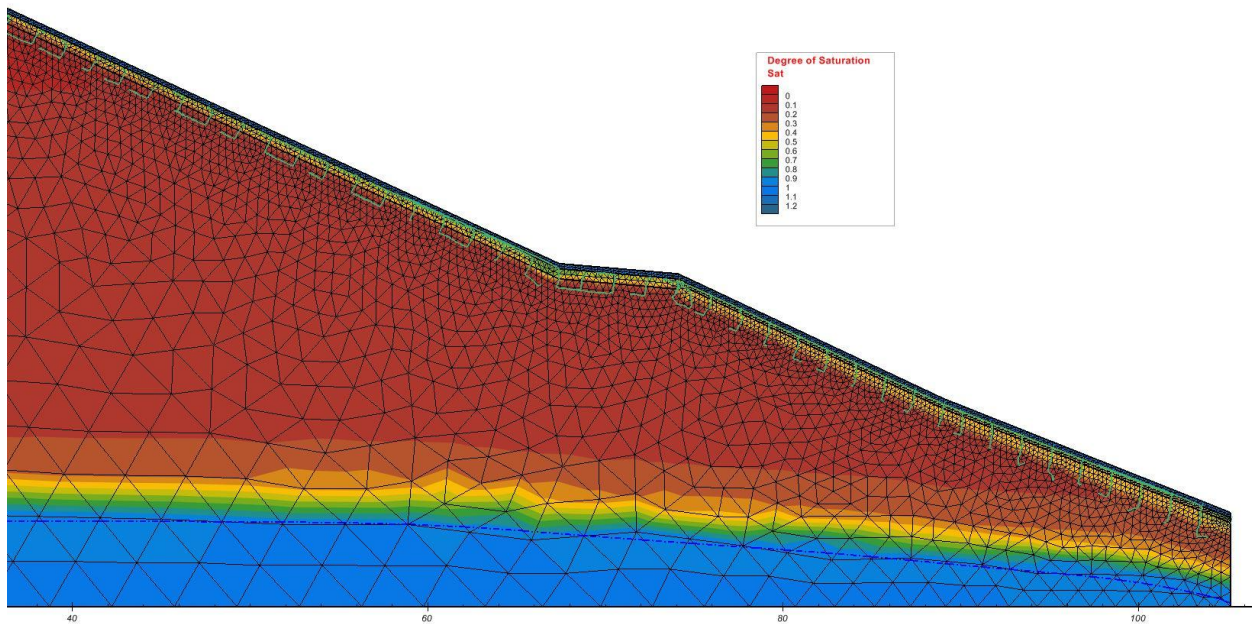


Figure 16. Day 3-Conventional Planar Slope (Ditch G) saturation with streamlines

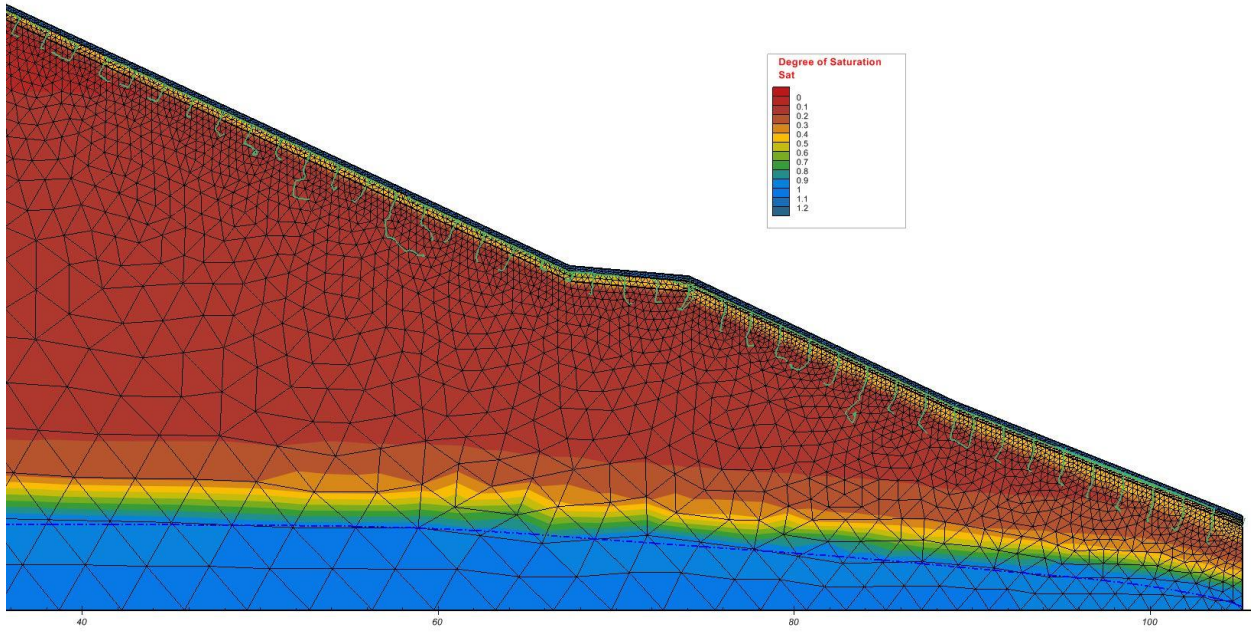


Figure 17. Day 4-Conventional Planar Slope (Ditch G) saturation with streamlines

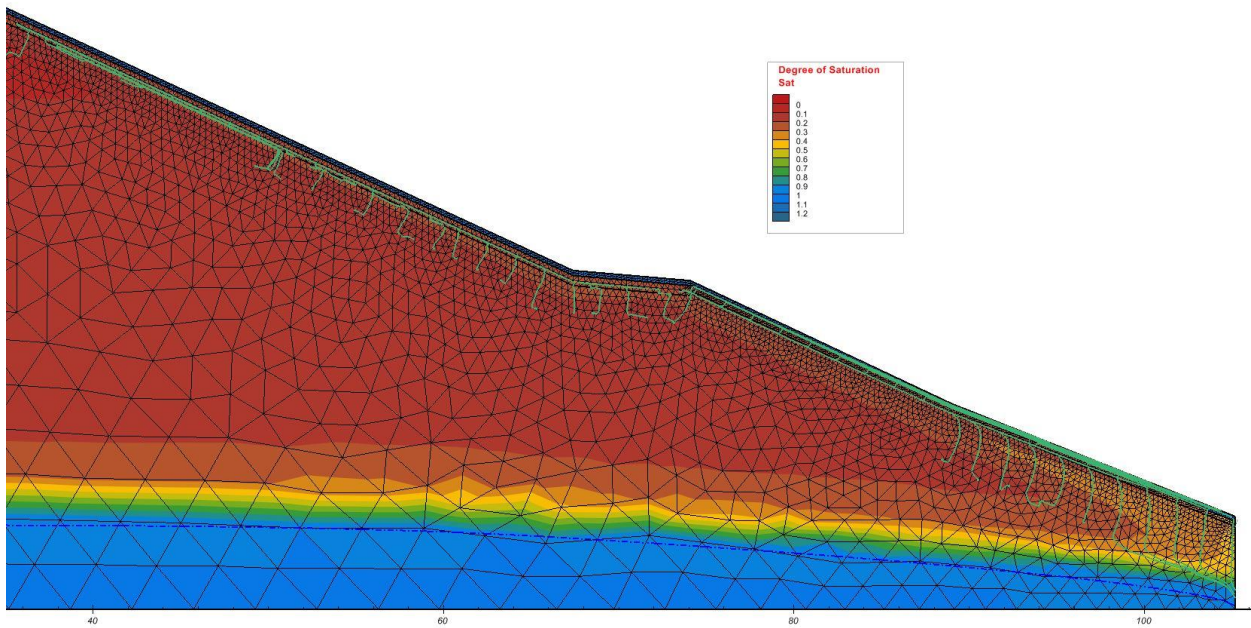


Figure 18. Day 15-Conventional Planar Slope (Ditch G) saturation with streamlines

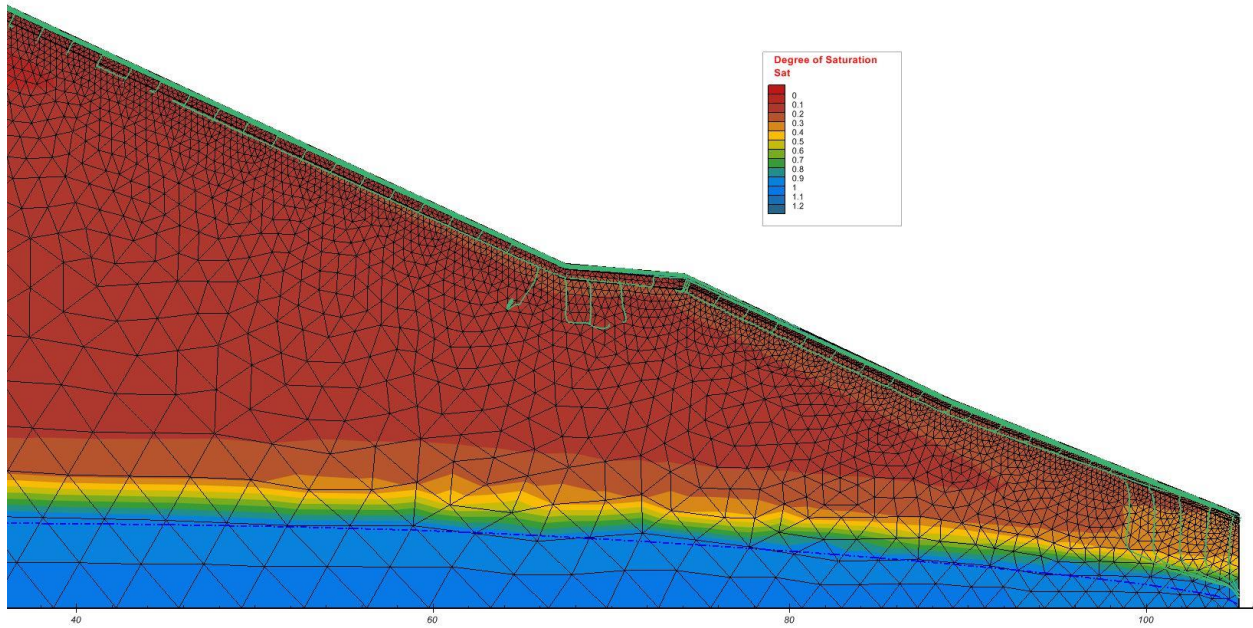


Figure 19. Day 25-Conventional Planar Slope (Ditch G) saturation with streamlines

On day 3 the growth layer is at 100% saturation, while the growth layer is at 40 to 50 percent saturation 48 hours after the storm has occurred. Saturation is starting to build up at the toe of slope, which is an indication of pore-pressure build-up. Streamlines are able to form due to 50% saturation in the barrier. Day 4 is similar in saturation with the growth layer still completely saturated and the streamlines are starting to get larger as the saturation in the barrier increases. The streamlines are gaining magnitude at the downslope toward the toe. On day 20, the growth layer is still completely saturated, but the hydraulic barrier has decreased back to $S=20$ to 30% . There is still more saturation at the toe of the slope which is expected since the toe is closer to the phreatic surface. The streamlines can only be seen near the toe of the slope and the downslope to the bench. On the last day (day 25), the growth layer remains completely saturated, but the hydraulic barrier has almost completely desaturated. The desaturating of the barrier as time passes causes more water to pass from the barrier into the fill. The saturation in the barrier is only 15 to 20% saturation, and the streamlines only exist at the bench and toe of the planar slope. The conventional planar slope also has no issues with mesh generation issues within the model.

Geomorphic Slope (GLD-C) Saturation and Streamlines

Figures 20 to 23 show the saturation of the geomorphic slope before and after the storm event. Table 22 shows helps to identify the saturation on each corresponding day.

Table 22. Saturation of growth layer and hydraulic barrier

Geomorphic Channel-C		
Day	Growth Layer Saturation (%)	Hydraulic Barrier Saturation (%)
3	100	50
4	100	60
15	100	30 to 35
25	100	20 to 25

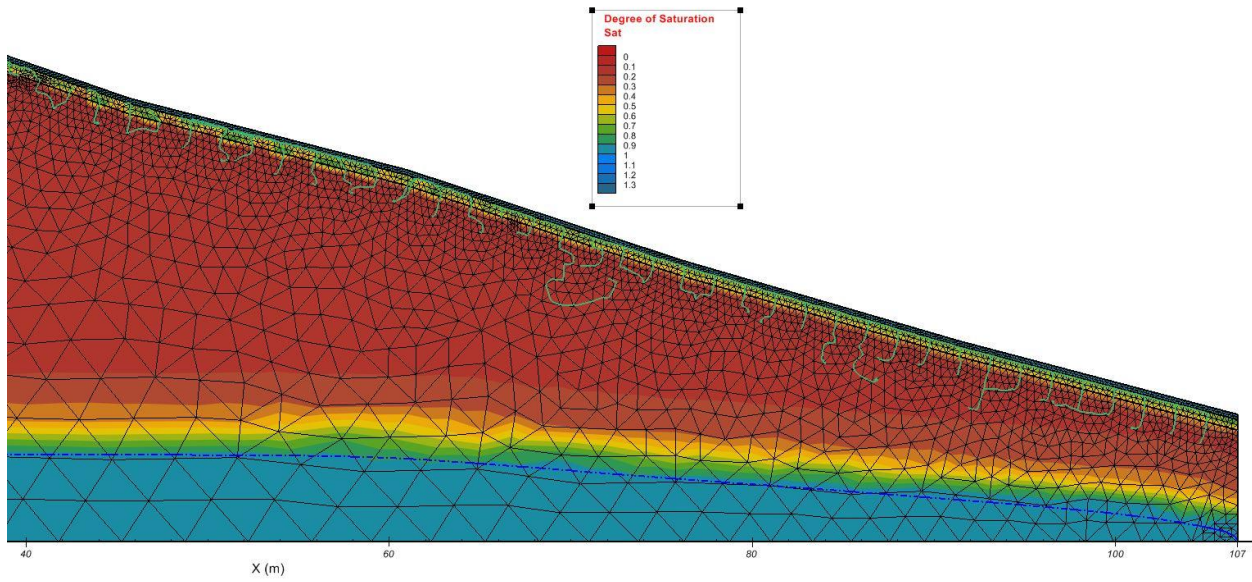


Figure 20. Day 3-Geomorphic Slope (GLD-C) saturation with streamlines

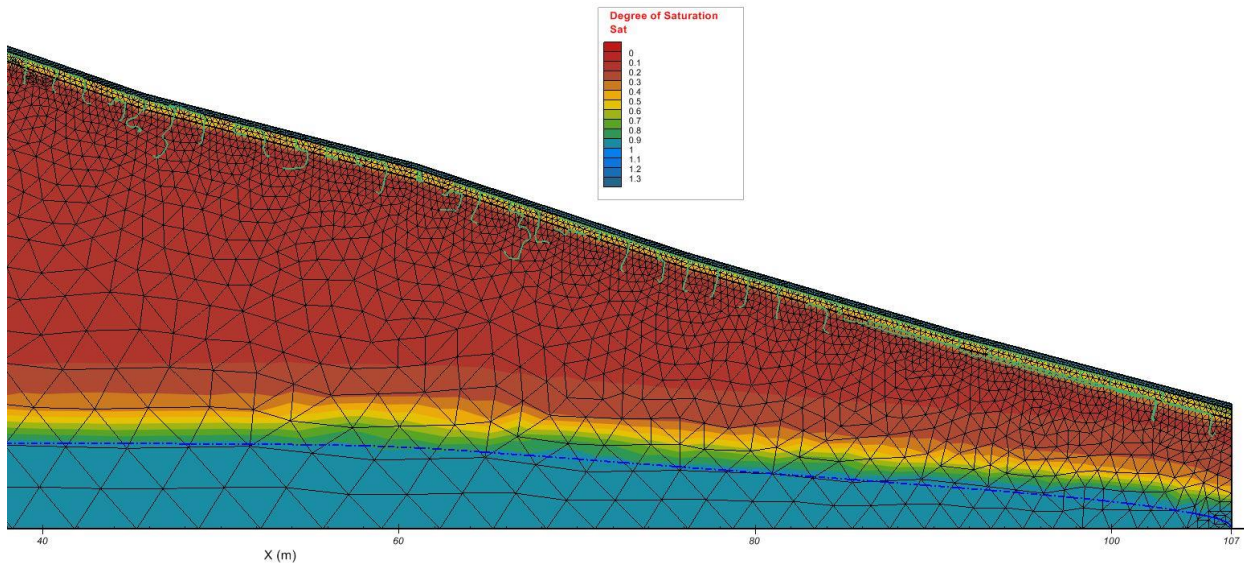


Figure 21. Day 4-Geomorphic Slope (GLD-C) saturation with streamlines

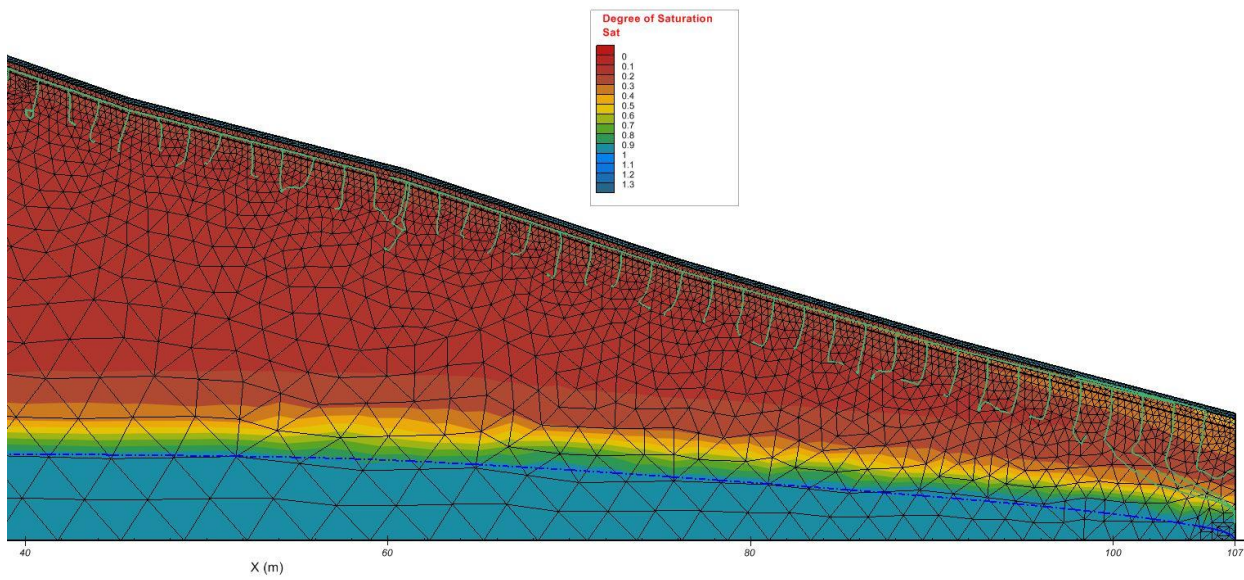


Figure 22. Day 15-Geomorphic Slope (GLD-C) saturation with streamlines

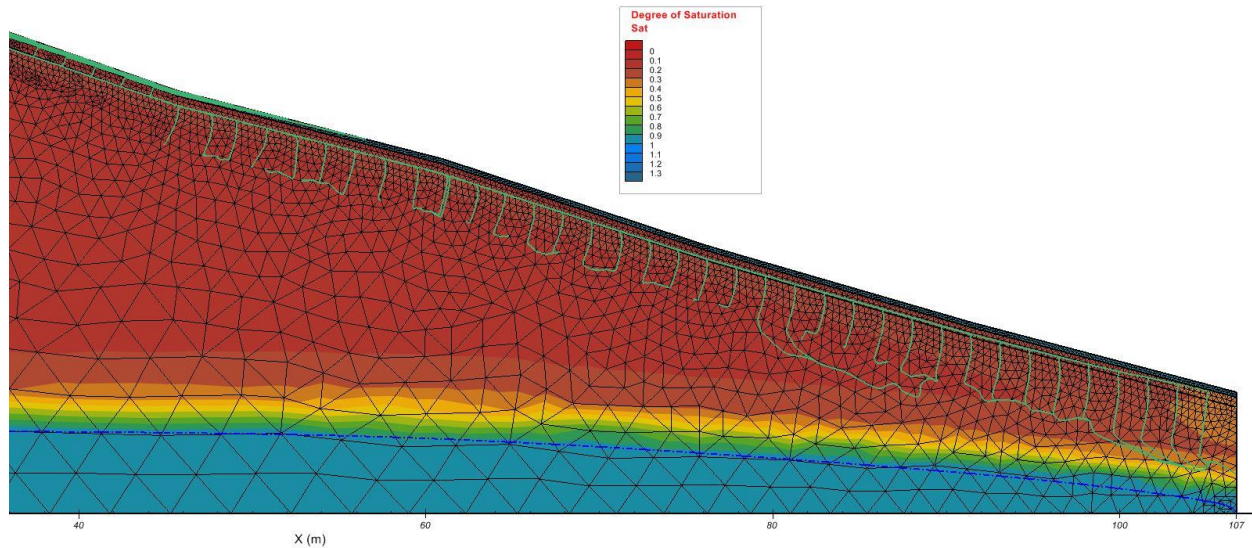


Figure 23. Day 25-Geomorphic Slope (GLD-C) saturation with streamlines

On day 3, 48 hours after the storm occurrence; the growth layer has reach 100% saturation, and the hydraulic barrier is at S=50% similar to the conventional planar slope. There is no evidence of increased saturation at the toe of the slope. Streamlines are starting to generate with saturation at 50% in the barrier. Day 4 shows that the growth layer remains fully saturated and the hydraulic barrier has reached 60% saturation. There is still no change of saturation at the toe of the slope indicating a pore-pressure build-up that was evident in the conventional planar slope saturation. The day 4 streamlines are more prevalent up the slope than at the toe. As time continues to Day 15, the hydraulic barrier has desaturated to 30 to 35% saturation. The growth layer remains at 100% saturation. The toe of the slope is starting to have increased saturation, which indicates a build-up in pore pressure. The streamlines on Day 15 are also much more prevalent as desaturation occurs, which is expected. The last day (Day 25), shows that the growth layer remained fully saturated throughout the model. The growth layer staying fully saturated throughout 25 days is a sign that growth is capable, and a root matrix can form. Saturation in the hydraulic barrier has decreased to 20 to 25%, and the streamlines are only forming on the downward 2/3rd's of the slope profile, meaning the water is draining down the slope and ponding is not occurring.

Seepage/Stability Analysis

As mentioned previously, after the seepage was simulated, it was then coupled with a slope stability analysis according to General Limit Equilibrium (GLE). By doing the seepage coupled with stability, a worst-case factor of safety could be attained. A flux line was inserted on both conventional planar and geomorphic profiles to track infiltration from the hydraulic barrier into the fill material. For the conventional planar slope, the flux line was inserted at the bench (67.4, 19.2 m) and was ended at the toe of the slope (105.2, 4.4 m). For the geomorphic slope the flux line was inserted at the lower 2/3rd's of the profile (45.7, 24.5 m) and was also drawn to the

toe of the slope (106.7, 5.1 m). The flux lines were inserted at these two points where large amounts of seepage occur according to the saturation and streamline figures (Figures 16-23). Table 23 and 24 shows the quantitative results for the precipitation/infiltration, and its corresponding factor of safety for the conventional planar and geomorphic slopes. The infiltration rates are for the cumulative model duration. The tables also show quantitative results done by another researcher doing a similar study on the same slope profiles (Stevens, 2016). Figures 24 and 25 shows where the critical failure occurs and its corresponding mean factor of safety.

Table 23. Quantitative seepage/stability analysis for conventional planar slope (Ditch G)

Conventional Planar Slope (Ditch G)						
Growth Layer	Hydraulic Barrier Thickness	Volume Precipitation	Infiltration	LCV Stability	Mean Stability	HCV Stability
% by volume	meters (feet)	m ³	m ³	FS	FS	FS
80/20	0.6 (2)	15.59	2.66	1.53	1.64	1.76
60/40	0.6 (2) (Stevens, 2016)	18.11	8.25	N/A	1.30	N/A

Table 24. Quantitative seepage/stability analysis for geomorphic slope (GLD-C)

Geomorphic Slope (GLD-C)						
Growth Layer	Hydraulic Barrier Thickness	Volume Precipitation	Infiltration	LCV Stability	Mean Stability	HCV Stability
% by volume	meters (feet)	m ³	m ³	FS	FS	FS
80/20	0.6 (2)	15.37	5.92	2.08	2.12	2.15
60/40	0.6 (2) (Stevens, 2016)	15.57	6.92	N/A	1.70	N/A

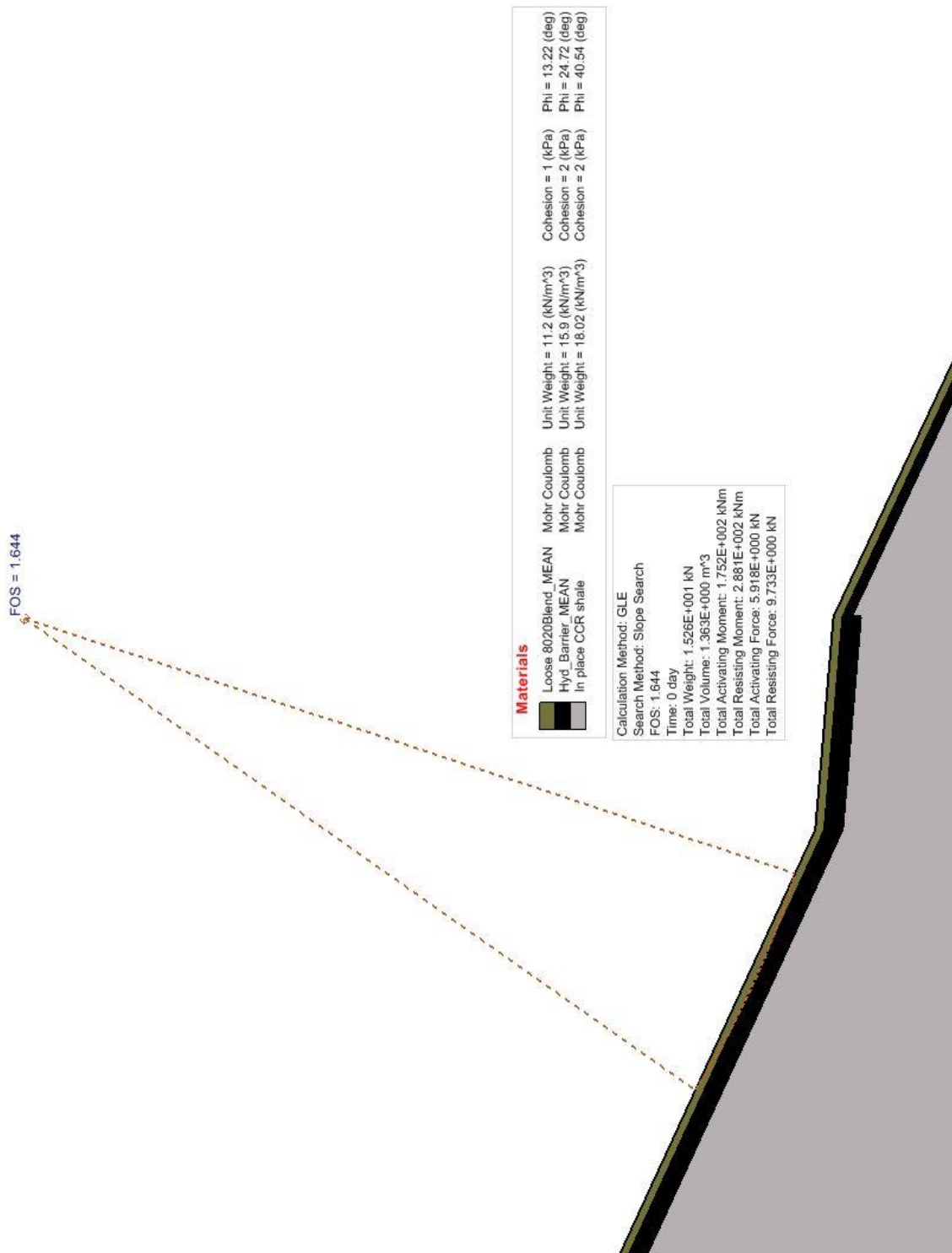


Figure 24. Mean factor of safety/critical area for conventional planar slope (Ditch G)

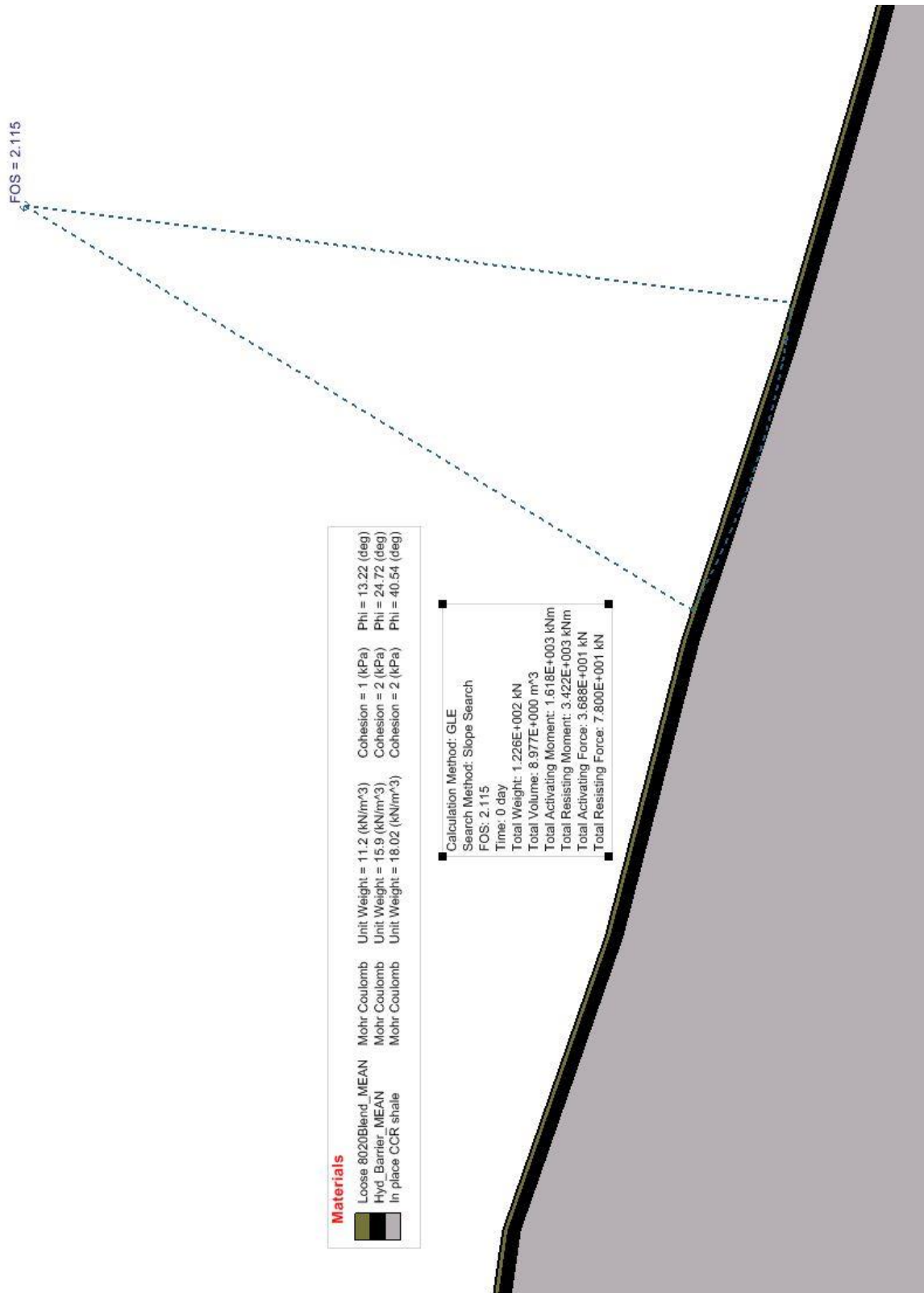


Figure 25. Mean factor of safety/critical area for geomorphic slope (GLD-C)

Conventional Planar Slope (Ditch G) Conclusions

1. Table 23 shows that the model simulated by Stevens (2016) had 2.52 m³ more of precipitation than the model simulated for this research. This could be attributed to a different boundary condition for the 100-year storm.
2. A large decrease in infiltration is also noted between Stevens (2016) and the model simulated for this research. The model for this research had a 5.59 m³ decrease in infiltration. This is due to a 50% reduction of MGroTM in an 80/20 growth layer compared to a 60/40 growth layer. The 80/20 layer allows less water to be retained in the MGroTM, which could then leach into the barrier and fill material during desaturation.
3. The large reduction in infiltration also leads to an increased mean factor of safety (1.64). The 1.30 factor of safety is due to the large volume (8.25) of infiltration (Stevens. 2016).
4. The LCV factor of safety shows that even under lesser friction angle values, the slope remains stable with a FS=1.53, which greater than FS=1.50, which is recommended by Superfesky and Michael (2007).
5. Figure 24 shows that the critical area of failure for the mean factor of safety occurs directly upslope from the bench. The critical area shows that the failure only occurs on the 80/20 growth layer and does not reach the hydraulic barrier. The reason the failure occurs here is due to sloughing, which is the loss of cohesion due to high saturation. The growth layer remains 100% saturated throughout the 25-day model.
6. Grass may be able to bind the structure together in a root matrix increasing the overall stability.

Geomorphic Slope (GLD-C) Conclusions

7. Table 24 shows that both studies had similar volumes of precipitation for the 100-year storm.
8. The 80/20 growth layer proved to decrease the infiltration by 1.00 m³ compared to 60/40 Stevens (2016). The 50% reduction in MGroTM allows less water to reside in the growth layer, and increase runoff towards the toe for the entire site.
9. The geomorphic slope with the 80/20 layer had a much higher factor of safety compared to Stevens (2016). A 0.42 increase in factor of safety can be attributed to a more competent hydraulic barrier. The hydraulic barrier had a friction angle ranging from 24.12 to 25.08 degrees compared to Stevens (2016) 43.21 to 44.96 degrees (Table 14). The friction angles that range from 43.21 to 44.96 were done according to a direct shear test compared to an ICU test.
10. The geomorphic slope also proved to have a much higher factor of safety compared (2.12) to the conventional planar slope (1.64). The reason for a large increase in factor of safety is due to the steepness of the conventional planar slope compared to the geomorphic slope.
11. Figure 25 shows that the critical area occurs in the middle of the slope profile. The middle of the geomorphic slope is where infiltration is occurring always throughout the

25-day model according to the streamlines in Figures 20 to 23. The critical area also breaks past the growth layer and into the hydraulic barrier, which is a major concern. The reason for failure to occur in the barrier is due to a large concentration of saturation greater than 50%.

12. The terrain profile also plays a role in the failure reaching the hydraulic barrier. There is no bench to alleviate driving forces that as there is in the conventional planar profile.
13. As mentioned in the conventional planar slope, a root matrix will form in the growth layer and may increase the overall stability. This may help the geomorphic slope from the failure breaking into the hydraulic barrier that is seen in Figure 25.

Conclusions and Recommendations

From the geotechnical investigation to the Finite Element Modeling, the conventional planar and geomorphic slope profiles show that the major areas of concern for this proposed cap and cover design lie in the overall physical properties of the CCR and 80/20 CCR/MGro™ growth layers. The hydraulic barrier shows that it performs as expected in the modeling being able to decrease infiltration compared to the 60/40 layers. The CCR material also proves to be more competent in the 24.12 to 25.08 degrees area compared to the high 43.21 to 44.96 degrees (Table 14). This was shown in the modeling, giving higher factors of safety under a worst-case scenario. Some recommendations that can be taken into consideration are as follows:

1. It is recommended that an isotropic consolidated drained (ICD) test be run on the 80/20 and 60/40 growth layers as a check to see how much the friction angle would change between a ICU, ICD, and direct shear tests.
2. The geomorphic slope proves to be a more stable slope compared to conventional design. It has higher infiltration volumes for this research than the conventional planar slopes, but the factor of safety values show that it would be a more stable slope long term.
3. With higher infiltration values for the geomorphic slope, the failure was able to break into the hydraulic barrier. This was the case with the model without grass growing. With grass growing, a root matrix can form and bind the structure together making it more stable.
4. Grass growing, and the formation of a root matrix will also promote evapotranspiration for the entire site.
5. The 80/20 growth layer shows the ability to decrease infiltration compared to the 60/40 layer. The 50% reduction of MGro™ allows a lesser amount of water to reside in the growth layer and promote runoff towards the toe of the slope
6. Throughout the 25-day model of the conventional planar slope, large amounts of saturation were prevalent at the toe of the slope. This is expected, but could raise concern due to a slope blowout at the toe with increased pore-water pressure.
7. Implement rock drains at the toes of both slope profiles to reduce saturation/pore-water pressure build-up.
8. Complete more advanced modeling in seepage/infiltration of geomorphic and conventional planar slopes to see if there are any diminishing returns with either landform.
9. The 80/20 growth layer proves to be a viable growth layer for the cap and cover design. The 50% reduction of MGro™ compared to the 60/40 growth layer could also greatly save costs in the construction of the structure.

References

- Albuquerque, A.J.J., 1994, *Geoenvironmental Aspects of Coal Refuse-Fly Ash Blends*, M.S. Thesis, Virginia Polytechnic Institute and State University, Blacksburg, VA.
- Almes, R.G. and A. Butail, 1976, "Coal Refuse: Its Behavior Related to the Design and Construction of Coal Refuse Disposal Facilities," *Proceedings of the Seventh Ohio Valley Soils Seminar on Shales and Mine Wastes*, Lexington, KY.
- ASTM Designation D422. (2007). "Standard Test Method for Particle-Size Analysis of Soils." *Annual Book of ASTM Standards*, American Society of Testing Materials, Easton, MD.
- ASTM Designation D698. (2007). "Standard Test Methods for Laboratory Compaction Characteristics of Soil Using Standard Effort (12400 ft-lbf/ft³ (600 KN-m/m³))." *Annual Book of ASTM Standards*, American Society of Testing Materials, Easton, MD.
- ASTM Designation D5084. (2010). "Standard Test Methods for Measurement of Hydraulic Conductivity of Saturated Porous Materials Using a Flexible Wall Permeameter." *Annual Book of ASTM Standards*, American Society of Testing Materials, Easton, MD.
- ASTM Designation D4767. (2011). "Standard Test Method for Consolidated Undrained Triaxial Compression Test for Cohesive Soils." *Annual Book of ASTM Standards*, American Society of Testing Materials, Easton, MD.
- Carpenter, A. F., & Fernandez, I. J. (2000). "Pulp sludge as a component in manufactured topsoil". *Journal of Environmental Quality*, 29(2), 387-397.
- Daniels, W.L., Haering, K., Evanylo, G., Burger J., & Beck, M. (2013). "Suitability of MeadWestVaco residuals for utilization as soil amendments on reclaimed mined lands and native soils" *Final Report Virginia Tech Department of Crop & Soil Environmental Sciences*
- D'Appolonia Consulting Engineers Inc, 2009. *Engineering and Design Manual Coal Refuse Disposal Facilities*, second ed. U.S. Department of Labor, Mine Safety and Health Administration [MSHA].
- Department of the Army, U.S. Army Corps of Engineers (2003). *Engineering and Design, "Slope Stability" Manual No. 1110-2-1902*.
- DePriest, Nathan C. (2015). "Assessing the conceptual design, groundwater movement, and contaminant desorption of geomorphic landform design as an alternative for conventional valley fill surface mine reclamation." *Doctoral Dissertation*, West Virginia University Morgantown, WV

- DePriest, N.C., Hopkinson, L.C., Quaranta, J.D., and Ziemkiewicz, P.F. (2015). "Geomorphic landform design alternatives for an existing valley fill in central Appalachia, USA: Quantifying the key issues." *Ecological Engineering*, 81, 19-29.
- Duncan, J. M. (2000). "Factors of safety and reliability in geotechnical engineering." *Journal of Geotechnical and Geoenvironmental Engineering*, 126(4), 307-316.
- Hegazy, Y. A., Cushing, A. G., & Lewis, C. J. (2004). *Physical, Mechanical and Hydraulic Properties of Coal Refuse for Slurry Impoundment Design. D'Appolonia Engineering, Monroeville, PA.*
- Koloski, J.W., Schwarz, S.D., Tubbs, D.W., *Geotechnical Properties of Geologic Materials, Engineering Geology in Washington, Volume 1, Washington Division of Geology and Earth Resources Bulletin, 78, 1989.*
- Laubenstein, J. (2004). "Beneficial use of short paper fiber (paper mill sludge) for pollution prevention in the mining industry." *TAPPI Paper Summit-Spring Technical and International Environmental Conference.*
- Lorimer, J.T. (2016). "Geomorphic Landform Design Principles Applied to an Abandoned Coarse Coal Refuse Pile on Steep Terrain in Central Appalachia". M.S. Thesis, West Virginia University, Morgantown, WV.
- Lu, Ning, and William J. Likos. *Unsaturated Soil Mechanics*. Hoboken, NJ: Wiley, 2004. Print.
- McCutcheon, H.P., 1983, *Liquefaction and Cyclic Mobility of Coal Refuse Material*, M.S. Thesis, Carnegie Mellon University, Pittsburgh, PA.
- Nicolau, J.M. (2003). "Trends in relief design and construction in opencast mining reclamation." *Land Degradation and Development*, 14, 215-226. DOI: 10.1002/ldr.54
- Russell, H., DePriest, N., and Quaranta, J.D. (2014). "Stability analysis comparison of conventional valley-fill to geomorphic landform designs." *Trans., Society of Mining Metallurgy and Exploration*, 336, 414-420.
- Saxena, S.K., D.E. Lourie and J.S. Rao, 1984, "Compaction Criteria for Eastern Coal Waste Embankments," *Journal of the Geotechnical Engineering Division, ASCE*, Vol. 110, No. GT2, pp. 262-284.
- Schor, H.J., and Gray, D.H. (2007). *Landforming: an environmental approach to hillside development, mine reclamation and watershed restoration*, John Wiley & Sons, Hoboken, NJ.

- Stevens, J.R., (2016). "Geotechnical testing and Finite Element Modeling of Geomorphic Landform Design with a Multi-Layer Cap and Cover System". West Virginia University, Morgantown, West Virginia, USA.
- Superfesky, M., Michael P. (2007). "Excess Spoil Minimization and Fill Stability." Proc., SME Annual Meeting, SME, Denver, CO, 1-13.
- Torres, G.H. (2011). "Estimating the soil-water characteristic curve using grain-size analysis and plasticity index." M.S. Thesis, Arizona State University, Tempe, AZ
- Toy, T.J., and Chuse, W.R. (2005). "Topographical reconstruction: a geomorphic approach." Ecological Engineering, 24, 29-35.
- Ward, Ken Jr. (2001, August 12). "A toxic legacy." Charleston Gazette-Mail. Retrieved from: <http://www.wvgazettemail.com/article/20010812/ARTICLE/308129998/>